Summer 8-31-2008

# On the rolling motion of viscous fluid on a rigid surface

Xinli Wang
*New Jersey Institute of Technology*

## ABSTRACT

## ON THE ROLLING MOTION OF VISCOUS FLUID ON A RIGID SURFACE

by
**Xinli Wang**

This thesis considers two closely related problems. First, the influence of insoluble surfactant at a moving contact line is considered. This work is mostly motivated by the air entrainment during the coating process where there is a three-phase contact point (e.g., air, liquid and solid). For moving contact line problems, when the fluid is assumed to be an incompressible Newtonian fluid and a no-slip boundary condition is enforced at the solid boundary, the non-integrable stress singularity arises at the contact line, which is physically unrealistic. The contact angle of $180^0$ is considered as a special case in which the singularity is absent. The previous work showed that there exists a non-singular local solution in the vicinity of the contact line for any capillary number. A simplified asymptotic model is used here to find a global solution with a $180^0$ contact angle. Also the effects of insoluble surfactant are checked and numerical results show there exists a critical capillary number above which there is no steady state solution.

The second problem is viscous droplets rolling down a non-wettable inclined plane. The recent experiments show that the contact angle is very large (close to $180^0$) when a droplet rolls on a super-hydrophobic surface. The biharmonic boundary element method (BBEM) is used to implement numerical simulations of rolling motion. The numerical results agree well with the experimental results and theoretical prediction. Numerical evidence is also found that the stress singularity at the contact line is alleviated with a $180^0$ contact angle. For droplets with insoluble surfactant on the surface, the finite volume method is used to track the evolution of

surfactant. It shows that the rolling motion is retarded because of Marangoni force due to nonuniform concentration distribution of surfactant.

# ON THE ROLLING MOTION OF VISCOUS FLUID ON A RIGID SURFACE

by
Xinli Wang

A Dissertation
Submitted to the Faculty of
New Jersey Institute of Technology and
Rutgers, The State University of New Jersey – Newark
in Partial Fulfillment of the Requirements for the Degree of
Doctor of Philosophy in Mathematical Sciences

Department of Mathematical Sciences, NJIT
Department of Mathematics and Computer Science, Rutgers-Newark

August 2008

## APPROVAL PAGE

## ON THE ROLLING MOTION OF VISCOUS FLUID ON A RIGID SURFACE

**Xinli Wang**

5/12/08

Michael Siegel, Dissertation Advisor — Date
Professor of Mathematics, NJIT

05/12/08

Michael Booty, Committee Member — Date
Associate Professor of Mathematics, NJIT

5/12/2008

Lou Kondic, Committee Member — Date
Associate Professor of Mathematics, NJIT

5/12/2008

Charles Maldarelli, Committee Member — Date
Professor of Chemical Engineering, City College of New York

5/12/2008

Demetrios Papageorgiou, Committee Member — Date
Professor of Mathematics, NJIT

## BIOGRAPHICAL SKETCH

**Author:** Xinli Wang

**Degree:** Doctor of Philosophy

**Date:** August 2008

**Undergraduate and Graduate Education:**

- Doctor of Philosophy in Mathematical Sciences,
  New Jersey Institute of Technology, Newark, NJ, 2008
- Master of Science in Applied Mathematics,
  New Jersey Institute of Technology, Newark, NJ, 2008
- Bachelor of Science in Applied Mathematics,
  Shandong University, Ji'nan, Shandong, China, 2000

**Major:** Mathematical Sciences

*To my entire family*

## ACKNOWLEDGMENT

I would like to thank my advisor Dr. Michael Siegel for his patient guidance and consistent encouragement. I have learned from him not only mathematical knowledge and logic way of thinking but also the optimistic and aspiring attitude to everyday life. Whenever I feel frustrated, he is always being there to encourage me and help me out. Without his help, this dissertation would not have been accomplished. In China, there is a saying that someone who is your teacher for one day will have been your parent for a whole lifetime. I would like to express my sincere thanks and gratitude to my advisor by this Chinese saying.

I would like to thank my committee members, Professor Demetrios Papageorgiou, Michael Booty, Lou Kondic and Charles Maldarelli for their kindness and advice in my research work. I am lucky that I have an opportunity to have them as my teachers in my Ph.D. study.

I would like to thank the Department of Mathematical Sciences for financial support during my stay at NJIT. I would also like to thank the Chinese Students and Scholars Association (CSSA) and the Office of International Students. They gave me a warm welcome as I begun my study in America.

I would like to express my gratitude to my friends Espin Leonardo and Qiming Wang for sharing experience of LaTeXand MATLAB. I would like to thank my classmates Anisha Banerjee, Lakshmi Chandrasekaran and Kamyar Malakuti who gave so much help to my wife and I when our baby was born. I would also like to thank the postdoc Svetlana Tlupova who gave me some advice for numerical calculations. I wish to extend my thanks to all the friends who gave me help during my life.

My deepest appreciation goes to my family. My wife, Bin Du gave her faith, understanding, love and support to me in my life. She also brought the best gift, my lovely daughter Anna Wang to this family during my Ph.D. study. My parents's

love and support are always there in my life, who are why I am pursuing my PhD. Without love from my family, it would be impossible to achieve this.

## TABLE OF CONTENTS

## TABLE OF CONTENTS
## (Continued)

**Chapter** **Page**

## LIST OF FIGURES

**Figure** **Page**

## LIST OF FIGURES
## (Continued)

**Figure** **Page**

## LIST OF FIGURES
## (Continued)

**Figure** **Page**

# CHAPTER 1

# INTRODUCTION

This work is partially motivated by air entrainment in the coating of an axisymmetric or three-dimensional fiber or two dimensional tape. The coating is a covering that is applied to an object to protect it or change its physical properties. An example would be a coating applied to an optical fiber to alter its index of refraction [37].

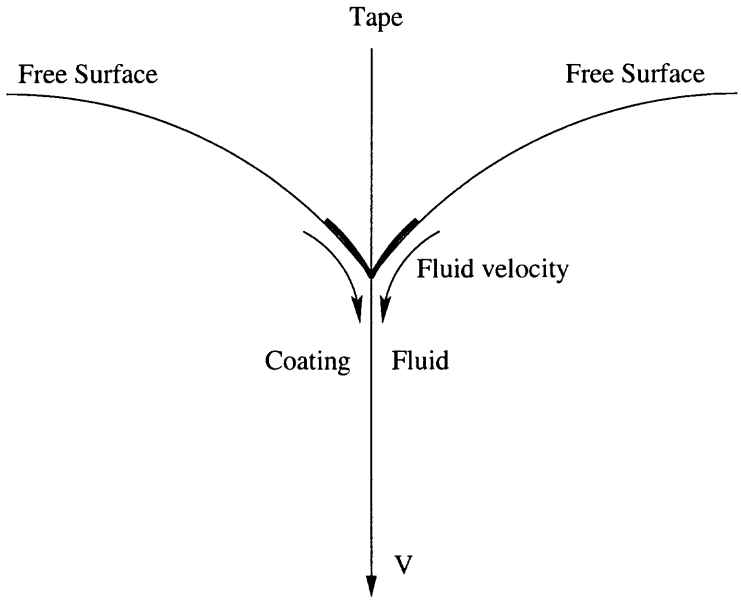


**Figure 1.1** Sketch of the tape coating. The heavy line refers to a stagnant layer of surfactant.

Figure 1.1 shows a schematic of tape or fiber coating. In the figure a tape is moving vertically downward into coating fluid and the speed of the tape is large enough so that the free surface deforms into a near cusp shape. Usually the tape can be coated uniformly when it is moved slowly. However, as the speed exceeds a critical value which depends on material and fluid properties, it is found that air can be entrained in the fluid in the form of tiny bubbles or long slender filaments of air that project

into the coating fluid [37]. These can ruin the coating because flaws in the form of bubbles, blemishes or voids appear in the coating on the tape or fiber surface. There has been some progress in understanding this entrainment process, but many questions remain.

Physical considerations suggest that surfactant can play an important role in the stability of the contact line and have an effect on the process of air entrainment. When surfactant is present on the free surface, the properties of the free surface change because of non-uniform distribution of surfactant (see e.g., [5, 16]). This results in a surface tension gradient, the Marangoni force, which can retard the fluid motion in the vicinity of the free surface. Suppose, for example, that a given surfactant has small or zero affinity for the coating material, i.e., the tape in figure 1.1, so that it piles up at the contact line. The accumulation of surfactant leads to a Marangoni force on the interface which opposes the downward tangential motion of the coating fluid adjacent to the free surface. When the fluid motion and interface shape are steady, and the surfactant is assumed to be insoluble and diffusion free, the Marangoni force completely retards the tangential flow at the interface, so that effectively a "no-slip" condition appears at points on the free surface where the surfactant concentration is nonzero. This is analogous to "stagnant cap" surfaces studied in [43]. Conversely, the fluid exerts a tangential force or drag on the steady interface. We hypothesize that, for sufficiently large downward tape velocity, the induced Marangoni force will not be large enough to counteract the drag on a steady state, no slip surface, and that this will lead to the nonexistence of a steady interfacial shape, and thus to an entraining flow.

There are several interesting issues related to this work. First of all, when the tape is immersed in fluid at high enough velocity, the free surface deforms into a near cusp shape near the contact line. The presence of a contact line makes mathematical modeling more complicated. A similar flow, but without complication of the contact

line, is the deformation of a free surface or inviscid bubble in a straining flow. Jeong and Moffatt [20] considered the deformation of a free surface in a two-dimensional flow acted by a vortex dipole in the figure 1.2. The undisturbed fluid occupies the

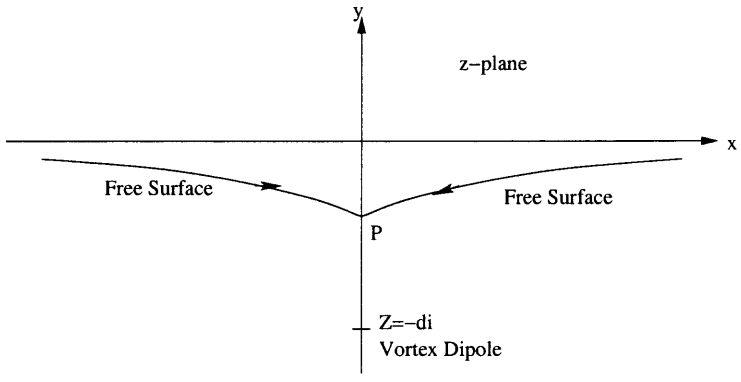


**Figure 1.2** Deformation of the free surface by a vortex dipole.

half-space $y < 0$ and a vortex dipole of strength $\alpha$ is placed at $z = -di$ ($z$ is a complex variable). Jeong and Moffatt used complex analysis and conformal mapping techniques to find an exact analytical solution for the steady shapes of the free surface, which exist for all finite capillary number $Ca_0 = \frac{\mu\alpha}{d^2\gamma}$, where $\mu$ is the viscosity and $\gamma$ is the surface tension. They also found that the curvature at $P$ on the free surface is proportional to $e^{32\pi Ca_0}$. Thus, although the steady shape is smooth for all finite $Ca_0$, it can have a very large curvature at $P$, which we refer to as a near cusp. Similar steady near cusp formation at the end of a bubble in a strain flow was found by Siegel [32]. The flow geometry considered by Siegel [32] is shown in Figure 1.3. Here a four-roller mill is filled with a highly viscous fluid and the rollers rotated in the directions shown, which produces a strain flow in the neighborhood of a bubble at the center of the mill. Exact analytical solutions were found for steady state shapes both with and without surfactant as well as for the time dependent evolution, for rather general far-field flows. In the case of certain nonlinear far-field flows produced by four rollers [2] and without surfactant, linearly stable steady state solutions exist for all capillary number defined as $Ca = \frac{2\mu GR}{\sigma_0}$, where $\mu$ is the viscosity of the outer fluid, $G$ is a parameter

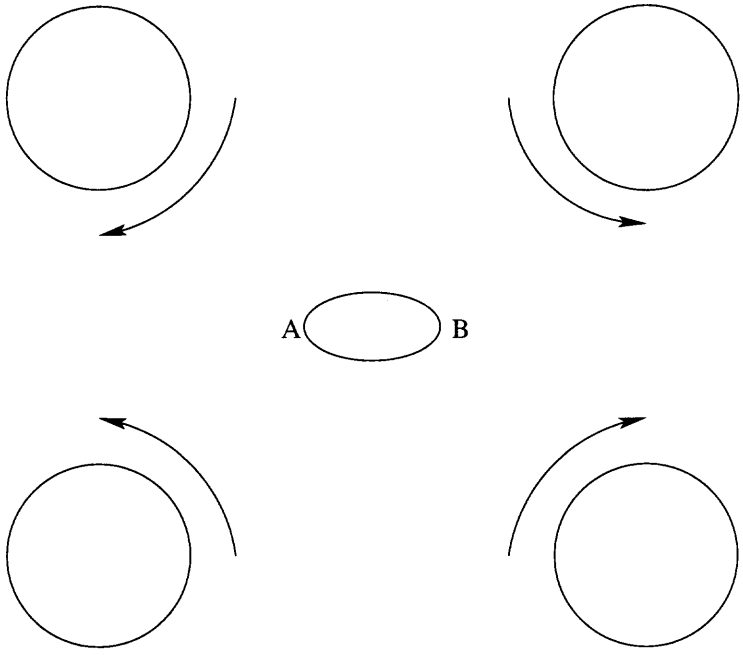


**Figure 1.3** An inviscid bubble in a two-dimensional model of Taylor's four roller mill.

characterizing the strain rate far from the drop, $R$ is the undeformed drop radius, and $\sigma_0$ is the surface tension. The curvature at the end points $A$ and $B$ is exponentially large in the capillary number, which is similar to the Moffatt's result. When insoluble, diffusionless surfactant is present, it piles up at the end points $A$ and $B$, and in the steady state, leads to a no-slip boundary condition near these points. The consequence of this was found to be that there is a critical capillary number $Ca_c$ above which no steady solution exists. Siegel [33] also generalized the exact solution to include the time dependence, and showed that in the presence of surfactant and for $Q > Q_c$, the free surface evolves into a transient cusp shape (i.e. with the infinite curvature). This is suggested to be related to tip-streaming [5] or entrainment. Booty and Siegel [28] studied the influence of insoluble surfactant on an inviscid axisymmetric bubble with a small aspect ratio involving in zero-Reynolds-number extensional flow. They find similar behavior, in that in absence of surfactant steady solutions exist for all $Q$, and with surfactant, there is a critical value $Q_c$ above which steady solutions no longer

exist. They also derived time-dependent solutions of asymptotic equations for $Q > Q_c$, which exhibited the tip-streaming behavior, which is analogous to air entrainment in the coating problem. These all motivate us to consider effect of surfactant on coating flow as shown in Figure 1.1.

What we are interested is how the contact line moves on a solid substrate if the no-slip boundary condition is enforced between the fluid and the solid substrate including at the contact line. The fluid is assumed incompressible and Newtonian. When this fluid displaces another immiscible fluid across a rigid solid, a nonintegrable stress singularity arises at the contact line [6], which is physically unrealistic. From a mathematical point of view, this singularity of the model comes from the velocity discontinuity at the contact line where, in the reference frame moving with the substrate, the solid substrate is at rest but the fluid near the contact line has to move. There are several proposed ways to remove this singularity. The one most commonly applied is to relax the no slip boundary condition [9, 26]. Another way which has received much less attention is to set the contact angle to $\pi$ [11,25]. In view of the importance of a nearly cusped interface morphology prior to air-entrainment in coating flows, as depicted in Figure 1.1, we are interested in this second way, i.e., setting the contact angle to $\pi$. Benny & Timson [11] (with a sign error corrected by Dussan [7]) and Mahadevan & Pomeau [25] showed that there exists non-singular local solution in the vicinity of the contact line for any capillary number. When surfactant is present at the fluid interface, we suspect that there is a critical capillary above which steady shapes no longer exist.

The rest of work is organized as follows. In chapter 2, we consider a simplified problem involving rolling motion of a viscous fluid onto a rigid surface to analyze the influence of surfactant on an air entrainment during coating processes. In chapter 3, we consider a viscous drop rolling down an inclined non-wettable plane. The boundary element method is applied to numerically study this problem. There have

been a number of numerical studies of drops and films moving down an inclined solid substrate. Most of them studied thin drops by the lubrication approximation. Clay and Miksis [34] used a lubrication approximation to study effects of insoluble surfactant on droplet spreading. They found that surfactant can increase the speed of the translation of thin droplets. In the absence of surfactant, Homsy and his coworkers [1] numerically studied a gravity driven two-dimensional viscous flow with a moving contact line by a boundary element method. The stress singularity at the contact line is regularized by a numerical slip boundary condition (i.e., effective slip due to the numerical discretization). Since the effective regularization or slip depends on the numerical grid spacing, the method [1] does not converge as the mesh spacing near the contact line decreases. In particular, they found in [1] that the maximum height of the profile increases linearly as the logarithm of the mesh size decreases. Zhang, Miksis, and Bankoff [18] considered the dynamics of a viscous drop moving along a substrate under the influence of shear flow in a parallel-walled channel by using the front-tracking numerical method. The no-slip condition at the bottom wall is relaxed by using a Navier-slip law so that the non-integrable stress singularity at the contact line is regularized. They showed that for small Reynolds and capillary number, steady state solutions are obtained; for large values of the parameters, the drop surface appears to rupture. However none of these has considered full numerical simulation of rolling drops with contact angles at or near $\pi$, and none have considered the influence of surfactant on such drop motion. Our particular interest is in developing numerical methods for nonwetting rolling drops where the stress singularity is removed by setting the contact angle to $\pi$. We compare our numerical results to the theoretical predictions by [25]. Chapter 4 gives the detail of a local analysis in the vicinity of the contact line with a contact angle of $180^0$. We found a mistake in Mahadevan & Pomeau's analysis [25]. The stream function in their analysis does not satisfy the Stokes equation if the leading order pressure is taken to be constant. However a local

parabolic shape in their analysis is consistent with the lubrication approximation which is conveniently applied in the numerical calculation. Benney & Timson [11] found a local non-singular solution for any capillary number. But the local shape is determined by the capillary number that makes it difficulty to be applied in the numerical calculation.

# CHAPTER 2

# MODEL PROBLEM FOR THE CONTACT ANGLE OF Π: THE FLOW IN A CHANNEL

## 2.1 Introduction

Entrapment of air bubbles during liquid-film coating can lead to flaws such as blemishes or voids. Recent experimental studies [37] suggest there is a connection between air entrainment in coating flows and tip streaming [5] - a phenomenon well known in emulsification technology in which interfacial contaminants (surfactants) can play an important role. This motivates us to examine, via simplified mathematical models, the influence of surfactant on air entrapment during coating processes.

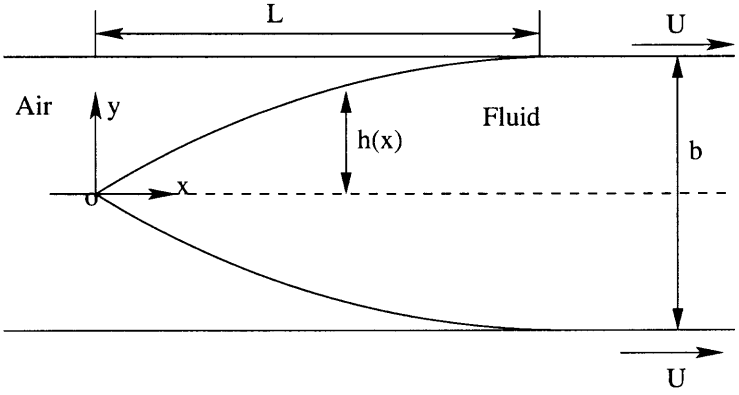


**Figure 2.1** The sketch of the flow in a channel.

We consider the Stokes flow in a channel with boundaries moving at speed $U$ (Figure 2.1). A fluid is assumed to eject from a source point $O$ and be bounded by the moving boundaries and free surfaces, and insoluble surfactant is present at the interface. The distance between two boundaries is $b$, and the length from the source point $O$ to the contact line where the fluid first meets the boundary is $L$. The outside region could be air or vacuum. The height of the free surface from the axis (dash line) is $h(x)$. We assume the flux of flow is constant. The contact angle at the contact line

is assumed to be $\pi$ which means the free surface is tangent to the solid substrate. The contact angle at the source point $O$ could be any angle. The origin of the Cartesian coordinates is at the source point $O$, and the $x$-axes is on the axis (dash line).

## 2.2 Governing Equations

The fluid considered here has a large viscosity $\mu$, so the flow motion is governed by the Stokes equations

$$\begin{aligned} \mu(u_{xx} + u_{yy}) &= p_x, \\ \mu(v_{xx} + v_{yy}) &= p_y, \\ u_x + v_y &= 0, \end{aligned} \tag{2.1}$$

where $p$ is the pressure and $u$ and $v$ are $x$ and $y$ components of fluid velocity respectively.

Then we consider the boundary conditions at the free surface. First we introduce the notation $[f]_2^1 = (f)^1 - (f)^2$ that is used to describe the jump in quantities between region 1 and 2 that are separated by the interface. The fluids in the region 1 and 2 may be two different fluids (or a fluid and a hydrodynamically passive region, e.g., air). In this problem, region 1 is vacuum and region 2 is occupied by fluid. The tangential stress is balanced by the Marangoni force because of non-uniform distribution of surfactant at the interface and the normal stress is balanced by the surface tension. The tangential stress balance (TSB) is:

$$[\overrightarrow{t} \cdot T \cdot \overrightarrow{n}]_2^1 = -\nabla_s \sigma \cdot \overrightarrow{t} \tag{2.2}$$

and the normal stress balance (NSB) is:

$$[\overrightarrow{n} \cdot T \cdot \overrightarrow{n}]_2^1 = \sigma\kappa \tag{2.3}$$

where $\overrightarrow{n}$ is a unit normal vector pointing into region 1, $\overrightarrow{t}$ is a unit tangential vector, $T$ is the stress tensor, and $\kappa$ is the curvature of the surface which is defined to be

positive for convex shapes, $\nabla_s = \nabla - \vec{n}(\vec{n} \cdot \nabla)$ is the surface gradient operator [40], and $\sigma$ is surface tension which depends on surfactant concentration $\Gamma$. In the two dimensional ($2D$) case,

$$\vec{n} = \frac{(-h_x, 1)}{\sqrt{1+h_x^2}}, \qquad \vec{t} = \frac{(1, h_x)}{\sqrt{1+h_x^2}}, \tag{2.4}$$

$$T_{ij} = -p\delta_{ij} + \mu(\frac{\partial u_i}{\partial x_j} + \frac{\partial u_j}{\partial x_i}). \tag{2.5}$$

Then the value at the right hand side in the equations (2.2) is

$$\nabla_s \sigma \cdot \vec{t} = \frac{\partial \sigma}{\partial s} = \frac{\sigma_x}{\sqrt{1+h_x^2}} \tag{2.6}$$

We assume a dilute concentration of surfactant, and employ a simple linear relationship between $\sigma$ and $\Gamma$ as the equation of state, i.e.,

$$\sigma = \sigma_0(1 - \frac{RT}{\sigma_0}\Gamma) \tag{2.7}$$

where $\sigma_0$ is the surface tension of the clean surface, $\Gamma_c$ is the concentration of surfactant at the contact point, $R$ is the universal gas constant, and $T$ is the absolute temperature.

The surfactant is considered to be insoluble, or confined to the air-fluid interface for which the steady-state equation in $2D$ is

$$\partial_s(u_s\Gamma) = D_s\Gamma_{ss}, \tag{2.8}$$

where $u_s$ is the surface velocity, $D_s$ is the surface diffusivity which is considered to be a constant on the fluid-air interface, and subindex $s$ of $\Gamma$ and $\partial$ refers to the derivative with respect to arc length $s$ along the interface. Equation (2.8) is assumed to hold at the wall as well, but with a different value of $D_s$ than at the interface. If we consider $\epsilon = \frac{b}{L} \ll 1$ , to the leading order the above equation (2.8) is equivalent to

$$\partial_x(u\Gamma) = D_s\Gamma_{xx}, \tag{2.9}$$

where $u$ is the $x$-component of the surface velocity.

At the contact point $A$, it is assumed that surfactant advects onto the solid boundary only from the free surface since the surfactant is considered to be insoluble i.e. there is no net flux of surfactant to and from the interface from the bulk flow. We assume the relative affinity of the surfactant for the boundary depends only on material properties of the surfactant and wall, e.g., not on velocity. At steady state, surfactant boundary condition at the contact point can be derived by integrating the equation (2.9) between a point $S$ on the interface and the contact point $A$ on the wall

.

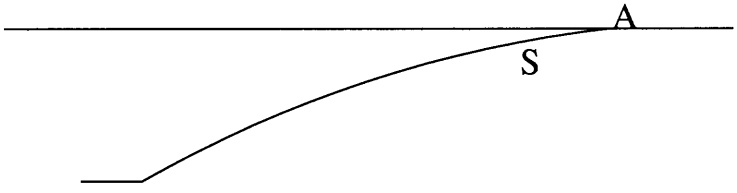


**Figure 2.2** The sketch of the contact region. $A$ is the contact point and $S$ lies on the surface.

$$\int_A^S \frac{d(u\Gamma)}{dx}dx = \int_A^S D_s\frac{d^2\Gamma}{dx^2}dx, \tag{2.10}$$

i.e.,

$$u(S)\Gamma(S) - u(A)\Gamma(A) = D_s(S)\frac{d\Gamma(S)}{dx} - D_s(A)\frac{d\Gamma(A)}{dx}, \tag{2.11}$$

where $D_s(A)$ is the diffusivity of the solid boundary which is assumed to be 0. It is further assumed that a certain proportion $\Lambda$ of surfactant accumulating at the contact point $A$ streams onto the solid boundary, which means $u(A)\Gamma(A) = U\Lambda\Gamma_c$ where $U$ is the velocity of the moving boundary and $\Gamma_c$ is the surfactant concentration at the

contact point. The parameter $\Lambda$ does not depend on the velocity and surfactant concentration at the contact line. It only depends on the material properties of the solid boundary. Then putting these two conditions into the above equation (2.11), finally we obtain the governing equation for the steady surfactant distribution at $x = S$:

$$u(S)\Gamma(S) - U\Lambda\Gamma_c = D_s\Gamma_x(S). \tag{2.12}$$

## 2.3 Exact Solution for No Flow

If the interface shape satisfies

$$b \ll L, \tag{2.13}$$

then lubrication theory can be applied to simplify the governing equations. We find the condition under which (2.13) holds by first seeking an exact solution in the case of no flow, i.e., both the inside fluid and the boundaries do not move. Because the flow is at rest, the pressure inside the fluid is constant (called hydrostatic pressure) and the fluid velocities are zero. In this case, the Stokes equations and the tangent stress balance equation are automatically satisfied. The normal stress balance is

$$-\sigma h_{xx} = p_0, \tag{2.14}$$

where $\sigma$ is surface tension, $h(x)$ is the equation of free surface, and $p_0$ is the constant hydrostatic pressure. The boundary conditions are

$$\begin{aligned} h(0) &= 0, \\ h(L) &= \frac{b}{2}. \end{aligned} \tag{2.15}$$

Solving the second order ordinary differential equation (2.14) with boundary conditions (2.15), we get the equation of the free surface:

$$h(x) = -\frac{p_0}{2\sigma}x^2 + (\frac{b}{2L} + \frac{p_0 L}{2\sigma})x. \tag{2.16}$$

At the contact point $x = L$, we require the contact angle be $\pi$ which means $h^{'}(L) = 0$. This condition gives a restriction on the hydrostatic pressure:

$$\frac{p_0 L}{\sigma} = \frac{b}{L}. \tag{2.17}$$

We then use the following characteristic values to non-dimensionalize equation (2.2)

$$\epsilon = \frac{b}{L}$$
$$x = x^{'} L,$$
$$h = h^{'} \epsilon L,$$
$$p = p^{'} \epsilon \frac{\sigma}{L}.$$

After non-dimensionalizing and dropping primes, we get the exact solution of free surface with the contact angle of $\pi$:

$$h(x) = -\frac{x^2}{2} + x. \tag{2.18}$$

Note that if the hydrostatic pressure $p_0$ satisfies the equation (2.17) with $\epsilon = \frac{b}{L} \ll 1$, then the interface shape will be long and slender, and lubrication theory can be applied to simplify the governing equations. This is done below to compute the steady interface shape when the surface is coated with insoluble surfactant and the walls move with a constant speed $U$.

## 2.4 Asymptotic Solution

We non-dimensionlize the problem in the following way:

$$x^{'} = \frac{x}{L},$$

$$y^{'} = \frac{y}{\epsilon L},$$

$$h' = \frac{h}{\epsilon L},$$

$$u' = \frac{u}{U},$$

$$v' = \frac{v}{\epsilon U},$$

$$p' = \frac{pL}{\epsilon \sigma_0},$$

$$\Gamma' = \frac{\Gamma}{\Gamma_c},$$

where $L$ is the length from the outlet to the contact point, $U$ is the velocity of the moving boundaries, and $\sigma_0$ is the constant surface tension at a clean or surfactant-free interface and $\Gamma_c$ is a representative surfactant concentration. For the numerical computation of section 2.6, it is convenient to take $\Gamma_c$ equal to the surfactant concentration at the contact point between the interface and the moving walls. In this way, the surface tension equation (2.7) becomes $\sigma = 1 - \beta\Gamma$ where $\beta = \frac{RT\Gamma_c}{\sigma_0}$. After plugging all these characteristic values into the equations and dropping the primes, we obtain the following governing equations. The Stokes equations and incompressibility condition become

$$\epsilon^2 u_{xx} + u_{yy} = \frac{\epsilon^3}{Ca} p_x, \tag{2.19a}$$

$$\epsilon^2 v_{xx} + v_{yy} = \frac{\epsilon}{Ca} p_y, \tag{2.19b}$$

$$u_x + v_y = 0, \tag{2.19c}$$

where $Ca = \frac{\mu U}{\sigma_0}$ is the capillary number.

The rescaled stress balance boundary conditions (2.2) and (2.3) are given by

$$\frac{1}{1+\epsilon^2 h_x^2}[\epsilon h_x(v_y - u_x) + (\frac{1}{\epsilon}u_y + \epsilon v_x)(1 - \epsilon^2 h_x^2)] = -\frac{1}{Ca}\frac{\beta\Gamma_x}{\sqrt{1+\epsilon^2 h_x^2}}, \tag{2.20}$$

$$-\epsilon p + Ca\frac{2}{1+\epsilon^2 h_x^2}(\epsilon^2 h_x^2 u_x - h_x(u_y + \epsilon^2 v_x) + v_y) = \epsilon\frac{(1-\beta\Gamma)h_{xx}}{(1+\epsilon^2 h_x^2)^{3/2}}, \tag{2.21}$$

at the interface $y = h(x)$ (only the upper interface is considered, the lower interface shape follows from symmetry).

From (2.12), the dimensionless steady-state equation for the surfactant concentration is found to be

$$u\Gamma - \Lambda = \frac{1}{PeCa}\Gamma_x, \tag{2.22}$$

where $Pe = \frac{L\sigma_0}{\mu D_s}$ is the Peclet number and $u$is evaluated on $y = h(x)$.

In order to keep the influence of pressure and surfactant at leading order, we rescale

$$Ca = Ca_0\epsilon^3, \quad \beta = \beta_0\epsilon^2, \quad \text{and} \quad Pe = \frac{Pe_0}{\epsilon^3}. \tag{2.23}$$

Thus the leading order systems are:

Governing equations:

$$u_{yy} = \frac{1}{Ca_0}p_x, \tag{2.24a}$$

$$p_y = 0, \tag{2.24b}$$

$$u_x + v_y = 0. \tag{2.24c}$$

Boundary conditions are

$$\text{TSB:} \qquad u_y = -\frac{\beta_0}{Ca_0}\Gamma_x, \tag{2.25}$$

$$\text{NSB:} \qquad p = -h_{xx}, \tag{2.26}$$

at $y = h(x)$.

The dimensionless steady state equation for surfactant is :

$$u\Gamma - \Lambda = \frac{1}{Ca_0 Pe_0}\Gamma_x, \qquad \text{at} \quad y = h(x). \tag{2.27}$$

Next we are going to solve the leading order system and find the free surface shape $y = h(x)$. Starting with the equation (2.24b), we find out that the pressure $p$ is the function of $x$ and does not depend on $y$. Then integrate the equation (2.24a) twice with respect to $y$, and obtain

$$u = \frac{1}{2Ca_0}p_x y^2 + A(x)y + B(x), \tag{2.28}$$

where $A(x)$ and $B(x)$ are the functions of integration. According to the symmetry about $y$-axis, $A(x)$ is 0. Thus

$$u = \frac{1}{2Ca_0}p_x y^2 + B(x). \tag{2.29}$$

The constant $B(x)$ will be determined by the flux conservation. Assume the flux to be $q$, i.e.,

$$\int_{-h}^{h} u dy = q \tag{2.30}$$

which leads to

$$B(x) = \frac{q}{2h} - \frac{p_x h^2}{6Ca_0}. \tag{2.31}$$

Then the velocity $u$ at the interface will be

$$u = \frac{1}{2Ca_0}p_x h^2 + \frac{q}{2h} - \frac{p_x h^2}{6Ca_0}, \qquad \text{at} \quad y = h(x), \tag{2.32}$$

and

$$u_y = \frac{1}{Ca_0}p_x h, \qquad \text{at} \quad y = h(x). \tag{2.33}$$

From NSB equation (2.26), we get $p_x = -h_{xxx}$, then

$$u = -\frac{1}{3Ca_0} h_{xxx} h^2 + \frac{q}{2h} \qquad \text{at} \quad y = h(x), \tag{2.34}$$

and

$$u_y = -\frac{1}{Ca_0} h_{xxx} h \qquad \text{at} \quad y = h(x).. \tag{2.35}$$

Comparing the equation (2.25) with the equation (2.35), we obtain

$$h_{xxx} h = \beta_0 \Gamma_x. \tag{2.36}$$

Integrating the above equation (2.36), we obtain

$$\Gamma = \frac{h h_{xx} - \frac{h_x^2}{2} - C_1}{\beta_0}. \tag{2.37}$$

where $C_1$ is a constant of integration. If we know the condition of $h_{xx}$ at the contact point, then we will be able to determine $C_1$. Since we assume the contact angle to be $\pi$, then $h_x(L) = 0$. A summary of the boundary conditions at the contact point is given below:

$$\begin{aligned} h(L) &= \frac{1}{2}, \\ h_x(L) &= 0, \\ \Gamma(L) &= 1. \end{aligned} \tag{2.38}$$

Thus

$$C_1 = \frac{h_{xx}(L)}{2} - \beta_0. \tag{2.39}$$

Inserting $u$ from equation (2.34), $\Gamma$ from equation (2.37), and $\Gamma_x$ from (2.36) into the equation (2.27), we finally obtain the governing equation for the free surface,

$$(-\frac{1}{3Ca_0}h_{xxx}h^2+\frac{q}{2h})(\frac{hh_{xx}-h_x/2-C_1}{\beta_0})-\Lambda=\frac{1}{Ca_0Pe_0}\frac{h_{xxx}h}{\beta_0}, \tag{2.40}$$

which can be written in the form of

$$h_{xxx}=\frac{\frac{q}{2}(-C_1+hh_{xx}-\frac{h_x^2}{2})-\beta_0\Lambda h}{\frac{h^2}{Pe_0Ca_0}+\frac{h^3}{3Ca_0}(-C_1+hh_{xx}-\frac{h_x^2}{2})}. \tag{2.41}$$

The boundary conditions for this third order ODE are

$$\begin{aligned} h(L)&=\frac{1}{2},\\ h_x(L)&=0,\\ h(0)&=0. \end{aligned} \tag{2.42}$$

The contact angle $h'(0)$ at the outlet $x=0$ is determined from the solution of the boundary value problem (2.41) and (2.42), as is the outlet surfactant concentration $\Gamma(0)$.

Before the shooting method is applied to solve this problem numerically, we should notice that the flux constant $q$ can be determined. In order to solve the flux $q$, we first consider the equation (2.40) at the contact point $A$ where $u=-\frac{1}{3Ca_0}h_{xxx}h^2+\frac{q}{2h}=1$ and $\Gamma=\frac{hh_{xx}-h_x/2-C_1}{\beta_0}=1$, thus

$$1-\Lambda=\frac{1}{Ca_0Pe_0}\frac{h_{xxx}h}{\beta_0}. \tag{2.43}$$

Substituting $h_{xxx}$ from the above equation (2.43) into the equation (2.34), we obtain

$$q=\frac{Pe_0\beta_0(1-\Lambda)}{6}+1. \tag{2.44}$$

## 2.5 Exact Solution for Clean Surface

Here we consider a related special case of flow without surfactant. From the previous analysis, we know the leading order governing equations

$$u_{yy} = \frac{1}{Ca_0} p_x, \tag{2.45}$$

$$p_y = 0. \tag{2.46}$$

The tangential stress balance is

$$u_y = 0 \qquad \text{at} \qquad y = h(x), \tag{2.47}$$

and the normal stress balance is

$$p = -h_{xx} \qquad \text{at} \qquad y = h(x). \tag{2.48}$$

The velocity is same as that solved for flow with surfactant. The velocity equation (2.29) is

$$u = \frac{1}{2Ca_0} p_x y^2 + B(x). \tag{2.49}$$

Then the derivative of the velocity $u$ with respect to $y$ is

$$u_y = \frac{1}{Ca_0} p_x y. \tag{2.50}$$

According to the tangential stress balance – no shear, we know

$$p_x = 0 \qquad \text{at} \qquad y = h(x). \tag{2.51}$$

From the normal stress balance, we know

$$p_x = -h_{xxx}. \tag{2.52}$$

Therefore,

$$h_{xxx} = 0. \tag{2.53}$$

The boundary conditions for the shape of free surface are

$$h(0) = 0, \tag{2.54}$$

$$h(1) = \frac{1}{2}, \tag{2.55}$$

$$h'(1) = 0. \tag{2.56}$$

Thus the shape of free surface is

$$h(x) = -\frac{x^2}{2} + x. \tag{2.57}$$

This is the same shape as for no flow. The reason is that all normal stress balance caring about is the hydrostatic pressure.

## 2.6 Numerical Results

The effects of insoluble surfactant are examined numerically for the steady state motion. As the capillary number $Ca_0$ decreases, we can consider that the characteristic velocity $U$ decreases, and the solution will approach the exact solution for no flow or for flow without surfactant. The Figure 2.3 shows different surface shapes for different values of Capillary number $Ca_0$, and the Figure 2.4 is the close-up of the left one. The dash-dot line represents the free surface for $Ca_0 = 10$; the dot line represents the free surface for $Ca_0 = 1$; the dash line represents the free surface for $Ca_0 = 0.1$; the solid line represents the free surface for $Ca_0 = 0.01$; the empty circles represent the exact solution of free surface without flow. This numerical calculation in Figure 2.3 show exactly what we anticipated that the solid line (free surface for small Capillary number $Ca_0 = 0.01$) approaches the exact solution of free surface without flow.

Figure 2.5 shows that surfactant concentration is more uniform when the capillary number is small than that of a large capillary number. In Figure 2.5 the dash-dot line represents surfactant concentration at interface for $Ca_0 = 10$; the dot line represents surfactant concentration at interface for $Ca_0 = 1$; the dash line represents surfactant concentration at interface for $Ca_0 = 0.1$; the solid line represents surfactant concentration at interface for $Ca_0 = 0.01$. People usually use Peclet number $Pe$ (the ratio of convection to diffusion along the interface) to examine the effects of surfactant. Here we use Capillary number $Ca_0$ to examine the effects of surfactant, which in fact is equivalent to use Peclet number because the large Capillary number means strong convention along the interface. In Figure 2.5, the solid line (for the small Capillary number $Ca_0 = 0.01$) means when the convection along the interface is weak, the surfactant concentration is almost uniform. The dash-dot line (for the relatively large Capillary number $Ca_0 = 10$) means when the convection along the interface is relatively large, the amount of surfactant at $x = 1$ (at the contact line) is much larger than the amount of surfactant at $x = 0$ (at the outlet).

In Figure 2.5, empty circles at $x = 0$ represent the amount of surfactant at the outlet. We can see that the surfactant concentration at the outlet decreases as the capillary number increases. Finally the surfactant concentration is negative as the capillary number is very large in Figure 2.6 where we plot surfactant concentration at the outlet versus values of Capillary number $Ca_0$. This is physically unrealistic, which means there is no steady state solution. Thus there is a critical value for capillary number above which the steady state solution does not exist.

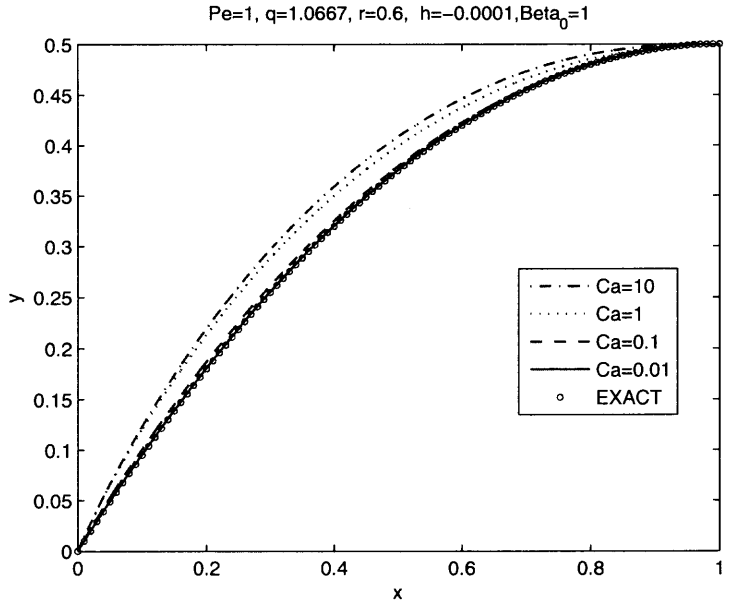


**Figure 2.3** Free surfaces for different values of the capillary number.

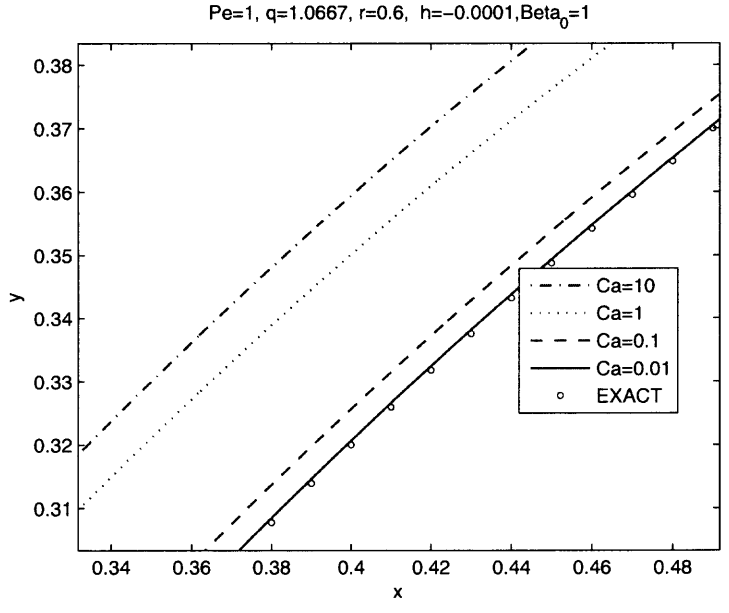


**Figure 2.4** Close-up of free surface for different values of capillary number.

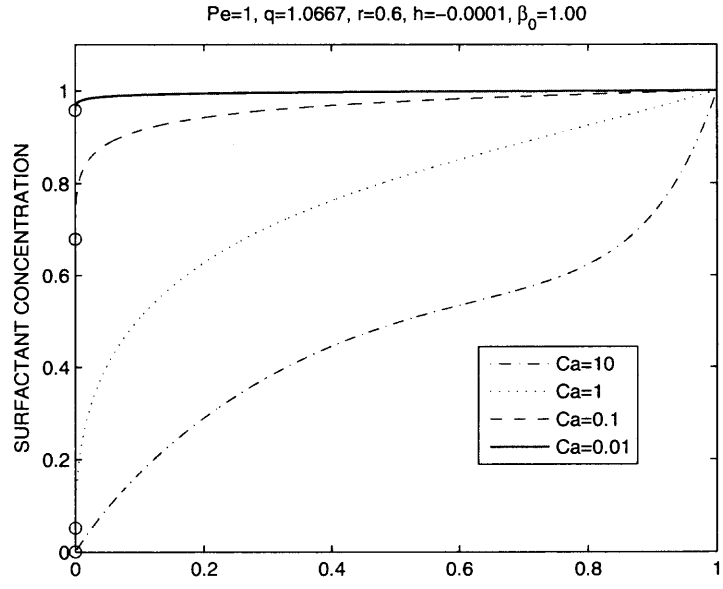


**Figure 2.5** The surfactant concentration varies as the capillary number varies.

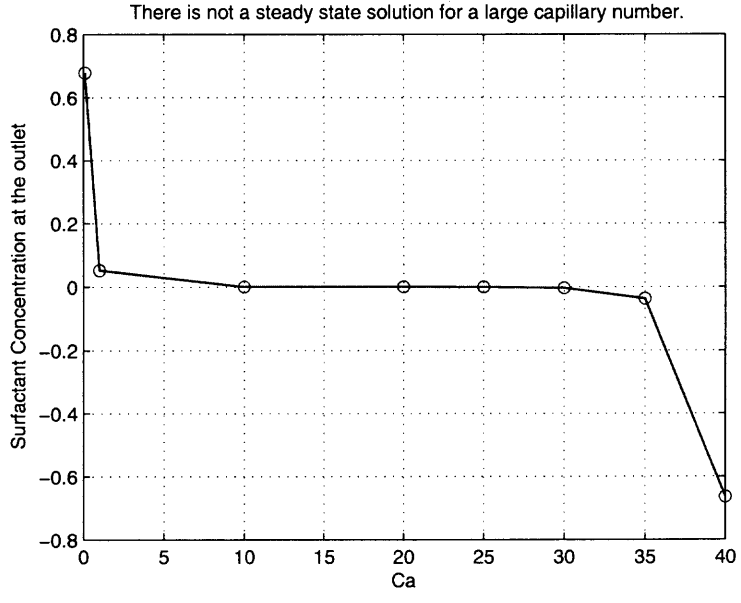


**Figure 2.6** The solution does not exist for large $Ca_0$. The first value of $Ca_0$ is 0.1.

# CHAPTER 3

# VISCOUS DROPS ROLLING ON A SUBSTRATE

## 3.1 Introduction

We consider the motion of viscus droplets on an inclined non-wettable plane which is a free surface problem with a moving contact line. Some researchers [9, 25] suggest that this movement has the form of a rolling or tank-treading motion instead of a sliding motion. Recent improvements in the fabrication of extremely rough surfaces have let to the creation of super-hydrophobic surfaces. Experiments show that a drop resting on a super-hydrophobic surface has a very large contact angle (near $180^0$). In the natural world, there are some plant leaves having super-hydrophobic properties [4, 45], such as lotus or water lily. Water droplets rolling on these leaves can carry away contaminating particles completely, resulting in a cleaned surface. It is called self-cleaning ability. Sliding water droplets are not effective at cleaning a surface. This self-cleaning effect is potentially useful in practical applications [27] such as waterproofing of clothes, anti-rain windshields and materials of very low friction in water, *etc.* David Quere and collaborators [8, 36] did some experiments of viscous drops rolling on an inclined non-wettable solid and showed some very interesting properties of rolling droplets in two different regimes: $(a)$ capillary force is dominant when the drop size is less than capillary length $(\frac{\sigma}{\rho g})^{1/2}$; $(b)$ the gravity is dominant when the drop size is larger than the capillary length $(\frac{\sigma}{\rho g})^{1/2}$ (where $\sigma$ is surface tension, $\rho$ is liquid density and $g$ is acceleration of gravity). Mahadevan and Pomeau [25] gave a theoretical prediction of the steady drop velocity by using a rough scaling analysis. We are interested in performing numerical computations to verify the conclusions of Mahadeven and Pomeaus scaling theory by using the boundary element method.

## 3.2 Governing Equations

Consider a region $\Omega$ of fluid separated by a surface $\partial\Omega$ from an inviscid or passive fluid. The fluid may also be in contact with a solid boundary as shown in Figure 3.1.

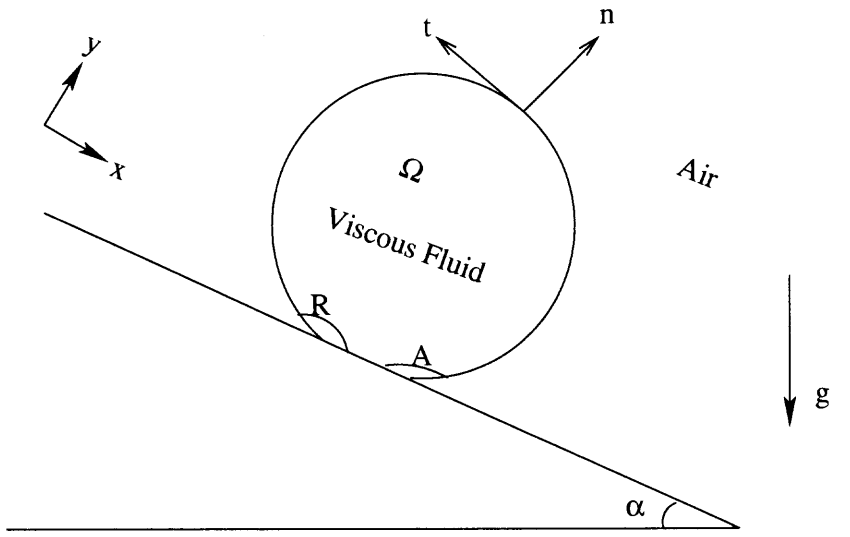


**Figure 3.1** A schematic of a drop rolling on an inclined plane. $\angle A$ is the advancing contact angle; $\angle R$ is the receding contact angle.

We assume the dynamics inside the drop is governed by the Stokes equations:

$$\nabla p = \mu \nabla^2 \mathbf{u} + \rho \mathbf{g}, \tag{3.1}$$

$$\nabla \cdot \mathbf{u} = \mathbf{0}, \tag{3.2}$$

where $\mathbf{u}(\mathbf{x}, \mathbf{y})$ is the fluid velocity, $p(x, y)$ is the pressure, $\rho$ is the density (assumed constant), $\mu$ is the viscosity and $\mathbf{g}$ is the acceleration of gravity.

On the free boundary separating $\Omega$ from passive fluid, there are three boundary conditions: kinematic condition; normal stress balance; tangential stress balance. The kinematic condition means fluid particles stay on the surface. The velocity $(u_x, u_y)$ of a point $P$ on the free boundary equals the velocity of the fluid particle at this point

$P$. This means that

$$\left.\frac{dx}{dt}\right|_{\partial\Omega} = \left.\frac{\partial\Psi}{\partial y}\right|_{\partial\Omega}, \qquad \left.\frac{dy}{dt}\right|_{\partial\Omega} = -\left.\frac{\partial\Psi}{\partial x}\right|_{\partial\Omega}, \tag{3.3}$$

where $u_x$ and $u_y$ are the components of velocity $\mathbf{u}(\mathbf{x},\mathbf{y})$, $\Psi$ is the stream function which satisfies

$$u_x = \frac{\partial\Psi}{\partial y}, \qquad \text{and} \qquad u_y = -\frac{\partial\Psi}{\partial x}, \tag{3.4}$$

and $\partial\Omega$ is the boundary. The stress balance conditions at the free surface are

$$t_j T_{ij} n_i = \frac{\partial}{\partial t_j}\sigma(\Gamma) \qquad \text{and} \qquad n_j T_{ij} n_i = -\sigma(\Gamma)\kappa, \qquad i,j = 1,2 \qquad \text{on } \partial\Omega, \tag{3.5}$$

where $T_{ij}$ is stress tensor

$$T_{ij} = -p\delta_{ij} + \mu\left(\frac{\partial u_i}{\partial x_j} + \frac{\partial u_j}{\partial x_i}\right), \tag{3.6}$$

$n_i$ is outward normal unit vector (i.e. pointed into the inviscid fluid), $t_i$ is the tangent unit vector oriented counter-clockwise, $\sigma(\Gamma)$ is the surface tension depending on the surfactant concentration and $\kappa$ is the curvature of the surface which is defined to be positive for convex surfaces. It is assumed without loss of generality that the constant pressure outside the drop is zero. On the other hand, these stress balance conditions can be written in the form:

Tangential Stress Balance (TSB):

$$\mu\left(\frac{\partial u_n}{\partial t} + \frac{\partial u_t}{\partial n}\right) = \frac{\partial}{\partial t}\sigma(\Gamma), \tag{3.7}$$

Normal Stress Balance (NSB):

$$-p + 2\mu\frac{\partial u_n}{\partial n} = -\sigma(\Gamma)\kappa, \qquad \text{on } \partial\Omega, \tag{3.8}$$

where $u_n$ and $u_t$ are the normal and tangential components of the velocity, and $\sigma(\Gamma)$ is surface tension which is the function of surfactant concentration $\Gamma$.

The governing equation for the surfactant concentration is a convection-diffusion equation [17]:

$$\frac{\partial \Gamma}{\partial t}|_s - \frac{\partial X}{\partial t} \cdot \bigtriangledown_s \Gamma + \bigtriangledown_s \cdot (\Gamma u_s) - D_s \bigtriangledown_s^2 \Gamma + \Gamma \kappa \mathbf{u} \cdot \mathbf{n} = \mathbf{0}, \tag{3.9}$$

where $t$ is time, $\bigtriangledown_s = \bigtriangledown - \mathbf{n}(\mathbf{n} \cdot \bigtriangledown)$ is the surface gradient [40], $u_s$ is the velocity vector tangent to the interface, $X(s,t)$ is a parametric representation of the interface, and $D_s$ is the surface diffusivity. Here we have considered the surfactant to be insoluble, i.e., there is no net flux of surfactant to and from the interface from the bulk liquid.

At the no-slip surface, the velocity of the fluid is equal to the velocity of the solid wall:

$$\mathbf{u}(\mathbf{x}, \mathbf{y}) = \mathbf{U_{wall}}. \tag{3.10}$$

### 3.3 Biharmonic Boundary Integral Method

There is a large body of literature on the biharmonic boundary integral method ( [15], [29], [30], [38], [39], [41]) solving free surface viscous flow problems. This method enables us to reformulate the original differential equations which hold on the entire fluid domain as integral equations on only the domain boundary. Thus we only need to discretize the boundary rather than the entire domain. This results in a significant reduction in computational effort. In the plane flow, we introduce the streamfunction $\Psi$ and the vorticity $\omega$.

$$u_x = \frac{\partial \Psi}{\partial y}, \qquad \text{and} \qquad u_y = -\frac{\partial \Psi}{\partial x}, \tag{3.11}$$

$$\omega = - \bigtriangledown \times \mathbf{u}. \tag{3.12}$$

Here we define the vorticity to be the negative curl of velocity. Then the Stokes equations can be written in the well-known form of:

$$\nabla^2 \Psi = \omega, \tag{3.13}$$

$$\nabla^2 \omega = 0. \tag{3.14}$$

By using the biharmonic boundary integral method, equations (3.13) and (3.14) can be rewritten as a coupled set of integral equations involving the streamfunction, vorticity, and their normal derivatives on the domain boundary ( [29], [30]).

$$\begin{aligned} \eta(p)\Psi(p) = &\int_{\partial\Omega} \left( \Psi(q) \frac{\partial G_1}{\partial n} - \frac{\partial \Psi(q)}{\partial n} G_1 \right) \partial\tilde{\Omega}(q) \\ &+ \frac{1}{4} \int_{\partial\Omega} \left( \omega(q) \frac{\partial G_2}{\partial n} - \frac{\partial \omega(q)}{\partial n} G_2 \right) \partial\tilde{\Omega}(q) \end{aligned} \tag{3.15}$$

$$\eta(p)\omega(p) = \int_{\partial\Omega} \left( \omega(q) \frac{\partial G_1}{\partial n} - \frac{\partial \omega(q)}{\partial n} G_1 \right) \partial\tilde{\Omega}(q) \tag{3.16}$$

where

1. $p \in \Omega + \partial\Omega, q \in \partial\Omega$.

2. $\partial\tilde{\Omega}(q)$ refers to the differential increment of $\partial\Omega$ at $q$.

3. $G_1$ and $G_2$ are given by

$$G_1 = \log|p-q| \qquad \text{and} \qquad G_2 = |p-q|^2(\log|p-q| - 1) \tag{3.17}$$

and are the fundamental solutions to

$$\nabla_p^2 G_1 = \delta(|p-q|) \qquad \text{and} \qquad \nabla_p^4 G_2 = \delta(|p-q|), \tag{3.18}$$

where $\nabla_p$ denotes the gradient with respect to $p$.

4. $\eta(p)$ is defined by

$$\eta(p) = \begin{cases} 0, & \text{if p} \notin \Omega + \partial\Omega \\ \theta, & \text{if p} \in \partial\Omega \\ 2\pi, & \text{if p} \in \Omega. \end{cases} \tag{3.19}$$

where $\theta$ is the internal angle included between the tangents to $\partial\Omega$ on either side of p. If the boundary $\partial\Omega$ is smooth, then $\theta = \pi$. The angle $\theta$ can take on other values at a three phase contact point where the free surface does not always smoothly connect with the solid substrate.

Now the governing equations only depend on the stream function, vorticity, and their normal derivatives. In order to define our problem in such a way that the whole system only depends on the four variables $\Psi$, $\frac{\partial\Psi}{\partial\mathbf{n}}$, $\omega$ and $\frac{\partial\omega}{\partial\mathbf{n}}$, we have to write the boundary conditions in terms of these quantities. Here we follow the derivation of the desired boundary equations from Betula [41] and Kuiken [15]. We first consider the tangential stress balance at the free surface. Substituting the following equations

$$u_n = \frac{\partial\Psi}{\partial t}, \qquad \text{and} \qquad u_t = -\frac{\partial\Psi}{\partial n} \tag{3.20}$$

into the tangential stress balance equation (3.7), we have

$$\frac{\partial^2\Psi}{\partial t^2} - \frac{\partial^2\Psi}{\partial n^2} = 0, \tag{3.21}$$

which holds on the boundary $\partial\Omega$. In addition, the vorticity at the contour is

$$\omega = \nabla^2\Psi = \frac{\partial^2\Psi}{\partial t^2} + \frac{\partial^2\Psi}{\partial n^2}. \tag{3.22}$$

We eliminate the second derivative with respect to the normal direction $\frac{\partial^2\Psi}{\partial n^2}$ using equation (3.21) to get the tangential stress balance condition,

$$-\omega + 2\frac{\partial^2\Psi}{\partial t^2} = 0. \tag{3.23}$$

Secondly, we consider the normal stress balance at the free surface. Substituting the normal velocity in terms of the streamfunction into the normal stress balance equation (3.8), we get

$$-p + 2\mu\frac{\partial}{\partial t}(\frac{\partial \Psi}{\partial n}) = -\sigma_0\kappa. \tag{3.24}$$

where the pressure $p$ is unknown. We use the governing Stokes equation to eliminate $p$. First differentiate the above equation (3.24) with respect to the tangential direction,

$$-\frac{\partial p}{\partial t} + 2\mu\frac{\partial^2}{\partial t^2}(\frac{\partial \Psi}{\partial n}) = -\sigma_0\frac{\partial \kappa}{\partial t}. \tag{3.25}$$

On the other hand, the tangential component of the governing equation is,

$$\begin{aligned}
\frac{\partial p}{\partial t} &= \mu \bigtriangledown^2 u_t + \rho g(t_x \sin\alpha - t_y \cos\alpha) \\
&= -\mu \bigtriangledown^2 \frac{\partial \Psi}{\partial n} + \rho g(t_x \sin\alpha - t_y \cos\alpha) \\
&= -\mu\frac{\partial}{\partial n} \bigtriangledown^2 \Psi + \rho g(t_x \sin\alpha - t_y \cos\alpha) \\
&= -\mu\frac{\partial \omega}{\partial n} + \rho g(t_x \sin\alpha - t_y \cos\alpha),
\end{aligned} \tag{3.26}$$

where the unit tangent vector is $(t_x, t_y)$ and the tilt angle is $\alpha$. The term $(t_x \sin\alpha - t_y \cos\alpha)$ is the dot product of the gravity vector and the tangent vector. It appears here because the coordinate system is set up in such a way that $x$ axis is parallel to the plane surface and $y$ axis is perpendicular to the plane surface, and then the unit direction of the gravity vector is $(\sin\alpha, -\cos\alpha)$. Comparing the above two equations (3.25) and (3.26) and eliminating $\frac{\partial p}{\partial t}$, we obtain

$$\frac{\partial \omega}{\partial n} + 2\frac{\partial^2}{\partial t^2}(\frac{\partial \Psi}{\partial n}) = -\frac{\sigma_0}{\mu}\frac{\partial \kappa}{\partial t} + \frac{\rho g}{\mu}(t_x \sin\alpha - t_y \cos\alpha). \tag{3.27}$$

It will be convenient in the numerical calculation to express the derivatives with respect to the tangent direction in terms of derivatives with respect to the contour

arc length $s$ [15, 21].

$$\begin{aligned} \frac{\partial}{\partial t} &= \frac{d}{ds}, \\ \frac{\partial^2}{\partial t^2} &= \frac{d^2}{ds^2} - \kappa \frac{\partial}{\partial n}. \end{aligned} \tag{3.28}$$

Then the tangential stress balance condition (3.23) is

$$-\omega + 2\frac{\partial^2 \Psi}{\partial s^2} + 2\kappa \frac{\partial \Psi}{\partial n} = 0. \tag{3.29}$$

The normal stress balance condition (3.27) is

$$\frac{\partial \omega}{\partial n} + 2\frac{\partial^2}{\partial s^2}\left(\frac{\partial \Psi}{\partial n}\right) - 2\frac{\partial}{\partial s}\left(\kappa \frac{\partial \Psi}{\partial s}\right) = -\frac{\sigma_0}{\mu}\frac{\partial \kappa}{\partial s} + \frac{\rho g}{\mu}(t_x \sin\alpha - t_y \cos\alpha). \tag{3.30}$$

Third, we consider the kinematic boundary condition through which we will determine how the fluid surface moves in time:

$$\begin{aligned} \frac{dx}{dt} &= u_x, \\ \frac{dy}{dt} &= u_y. \end{aligned} \tag{3.31}$$

Finally, we describe the boundary condition at the interface between a solid wall and the fluid. Here we use the no-slip condition which means the velocity of fluid is equal to the velocity of the solid wall.

$$u(x, y) = U_{\text{wall}}. \tag{3.32}$$

In all our calculations, the wall is rest $U_{\text{wall}} = 0$ where $U_{\text{wall}}$ indicates the velocity of the wall, which means:

$$\Psi = \text{const}, \qquad \text{and} \qquad \frac{\partial \Psi}{\partial n} = 0. \tag{3.33}$$

Without loss of generality, we let $\Psi = 0$ at the wall.

## 3.4 Numerical Method

We discretize the boundary polygonally into an N-gon and approximate the flow variables as being constant over each line of the N-gon. Here we consider all unknown values at the mid-points so that we can avoid calculating the flow values at the contact line. Then the governing equation can be written as the summations:

$$\begin{aligned}\eta_j\Psi_j = \sum_{i=1}^{N}\Bigg(&\Psi_i\int_{\partial\Omega_i}\frac{\partial G_1}{\partial n}\partial\tilde{\Omega} - \frac{\partial\Psi_i}{\partial n}\int_{\partial\Omega_i}G_1\partial\tilde{\Omega}\\ &+\frac{1}{4}\omega_i\int_{\partial\Omega_i}\frac{\partial G_2}{\partial n}\partial\tilde{\Omega} - \frac{1}{4}\frac{\partial\omega_i}{\partial n}\int_{\partial\Omega_i}G_2\partial\tilde{\Omega}\Bigg),\end{aligned} \tag{3.34}$$

$$\eta_j\omega_j = \sum_{i=1}^{N}\left(\omega_i\int_{\partial\Omega_i}\frac{\partial G_1}{\partial n}\partial\tilde{\Omega} - \frac{\partial\omega_i}{\partial n}\int_{\partial\Omega_i}G_1\partial\tilde{\Omega}\right), \qquad j = 1, 2, ..., N, \tag{3.35}$$

where the flow variables $\Psi_j$, $\frac{\partial\Psi_j}{\partial\mathbf{n}}$, $\omega_j$ and $\frac{\partial\omega_j}{\partial\mathbf{n}}$ are unknown variables, and the integrals of Green's functions and their derivatives can be evaluated analytically as discussed later. Then these two equations can be written in the form of matrix equations,

$$A\Psi + B\frac{\partial\Psi}{\partial n} + C\omega + D\frac{\partial\omega}{\partial n} = 0, \tag{3.36}$$

$$A\omega + B\frac{\partial\omega}{\partial n} = 0, \tag{3.37}$$

where $A$, $B$, $C$ and $D$ are matrices, and $\Psi$, $\frac{\partial\Psi}{\partial\mathbf{n}}$, $\omega$ and $\frac{\partial\omega}{\partial\mathbf{n}}$ are vectors [29, 30]. The elements of the matrices are

$$A_{ij} = \int_{q\in\partial\Omega_j}\frac{\partial}{\partial n}\log|p_i - q|\partial\tilde{\Omega}(q) - \eta_j\delta_{ij}, \tag{3.38}$$

$$B_{ij} = -\int_{q\in\partial\Omega_j}\log|p_i - q|\partial\tilde{\Omega}(q), \tag{3.39}$$

$$C_{ij} = \frac{1}{4}\int_{q\in\partial\Omega_j}\frac{\partial}{\partial n}[|p_i - q|^2(\log|p_i - q| - 1)]\partial\tilde{\Omega}(q), \tag{3.40}$$

$$D_{ij} = -\frac{1}{4}\int_{q\in\partial\Omega_j}[|p_i - q|^2(\log|p_i - q| - 1)]\partial\tilde{\Omega}(q). \tag{3.41}$$

where $\delta_{ij}$ is the Kronecker delta, i.e., $\delta_{ij} = 1$ if $i = j$, otherwise $\delta_{ij} = 0$. All these elements can be calculated analytically. We first define the following values in Figure 3.2:

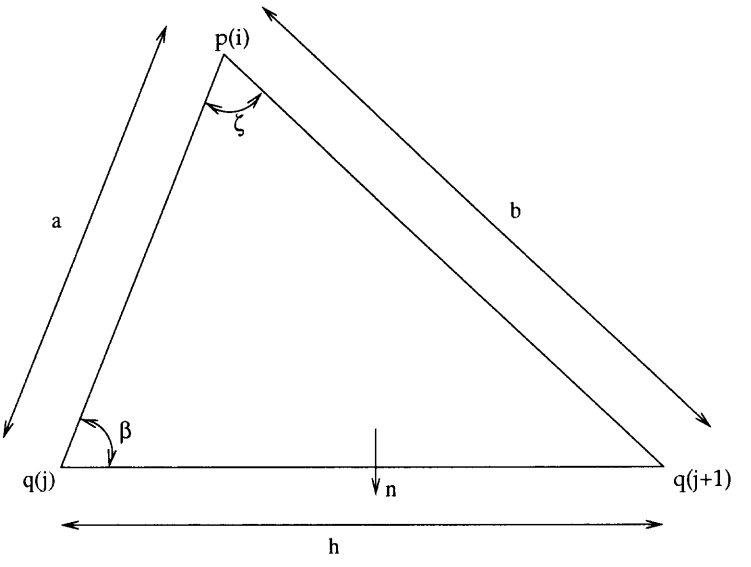


**Figure 3.2** Geometry for analytic calculation of integral on straight line segment. $p_i$ is a mid-point and $q_j$ is a node.

$$\begin{aligned} a &= |p_i - q_j|, \\ b &= |p_i - q_{j+1}|, \\ h &= |q_j - q_{j+1}|, \\ \beta &= \angle p_i q_j q_{j+1}, \\ \zeta &= \angle q_j p_i q_{j+1}. \end{aligned} \tag{3.42}$$

Then it is straightforward to calculate the integrals in equations (3.38) to (3.41).

$$\int_{q\in\partial\Omega_j} \frac{\partial}{\partial n} \log|p_i - q| \partial\tilde{\Omega}(q) = \zeta, \tag{3.43}$$

$$\int_{q\in\partial\Omega_j} \log|p_i - q| \partial\tilde{\Omega}(q) = a(\log a - \log b)\cos\beta + h\log b - h + a\zeta\sin\beta \equiv I, \tag{3.44}$$

$$\int_{q\in\partial\Omega_j} \frac{\partial}{\partial n}[|p_i - q|^2(\log|p_i - q| - 1)]\partial\tilde{\Omega}(q) = a(2I - h)\sin\beta, \tag{3.45}$$

$$\int_{q\in\partial\Omega_j}[|p_i-q|^2(\log|p_i-q|-1)]\partial\tilde{\Omega}(q)=$$
$$\frac{1}{3}[(h-a\cos\beta)^3(\log b-\frac{4}{3})+(a\cos\beta)^3(\log a-\frac{4}{3})]+(a\sin\beta)^2[I-\frac{2}{3}h-\frac{1}{3}a\zeta\sin\beta]. \tag{3.46}$$

So there are $4N$ unknown variables $\Psi, \frac{\partial\Psi}{\partial\mathbf{n}}$, $\omega$ and $\frac{\partial\omega}{\partial\mathbf{n}}$ corresponding to the discretization and $2N$ equations. The other $2N$ equations come from the normal and tangential stress balance conditions. The general centered second-order discretized derivative operators (see Appendix B) are used for these two equations. We write them in the form of matrix:

$$R\Psi+S\frac{\partial\Psi}{\partial n}+T\omega=0, \tag{3.47}$$
$$U\Psi+V\frac{\partial\Psi}{\partial n}+W\frac{\partial\omega}{\partial n}=b, \tag{3.48}$$

where $R$, $S$, $T$, $U$, $V$ and $W$ are $N\times N$ matrices. At the free surface, we have $R$ is a tridiagonal matrix, $S_{ij}=0$, $T_{ij}=-\delta_{ij}$, $V$ is a tridiagonal matrix as well and $W_{ij}=-\delta_{ij}$. $b$ is a vector containing the force of surface tension and the gravity. At the no-slip interface, assuming $U_{wall}=0$, we have $R_{ij}=1$ $V_{ij}=1$, $S_{ij}=0$, $T_{ij}=0$, $U_{ij}=0$, and $b_i=0$.

For a given initial shape, we can solve the following vector system by an LU decomposition.

$$\begin{pmatrix} A & B & C & D \\ 0 & 0 & A & B \\ R & S & T & 0 \\ U & V & 0 & W \end{pmatrix}\cdot\begin{pmatrix} \Psi \\ \frac{\partial\Psi}{\partial n} \\ \omega \\ \frac{\partial\omega}{\partial n} \end{pmatrix}=\begin{pmatrix} 0 \\ 0 \\ 0 \\ b \end{pmatrix}.$$

After solving the values of the stream function, vorticity, and their derivatives, the velocity field can be obtained by using the stream function and its normal derivative. Then the nodes are moved according to the kinematic boundary condition.

Simply we use the forward Euler approximation,

$$x(t+\Delta t) = x(t) + v_x \Delta t, \qquad \text{and} \qquad y(t+\Delta t) = y(t) + v_y \Delta t. \tag{3.49}$$

where $v_x$ and $v_y$ is the $x$, $y$ components of the velocity. These are not calculated directly from $v_x = \frac{\partial \Psi}{\partial y}$ and $v_y = -\frac{\partial \Psi}{\partial x}$, but rather are projected from the normal and tangential velocity which are evaluated directly from $v_n = \frac{\partial \Psi}{\partial t}$ and $v_t = -\frac{\partial \Psi}{\partial n}$, where the values of the stream function and its normal derivative are obtained from the numerical calculation. The reason that we do not use the derivative with respect to x and y is sometimes $\Delta x = 0$ or $\Delta y = 0$.

## 3.5 Validation of the Code

The code is validated by comparing with several exact solutions. The first problem is the free creeping viscous incompressible plane flow of a finite region, bounded by a simple smooth closed curve and driven only by surface tension. Hopper found an exact solution to this problem by using a time-dependent polynomial conformal mapping function to describe the coalescence of two cylinders [39]. The initial interface shape considered by Hopper is two tangentially touching cylinders, i.e., with two cusps. Our code cannot start from this initial shape with two cusps at $t = 0$. For the simplicity, we pick the initial time to be $t = 0.147$ where the cusps have become rounded. In Figure 3.3, the star indicates the initial shape at $t = 0.147$, the solid line indicates the exact solution at $t = 0.551$ and the dot indicates the numerical solution at $t = 0.551$. It shows Hopper's analytical solution and the numerically computed solution agree well at time $t = 0.551$.

In Figure 3.4 and 3.5, we apply the code to simulate the different initial shape reaching the steady shape. We start with a nephroid and an ellipse in Figure 3.4 and 3.5 respectively. Intuitively, the eventual steady shape would be a circle if the

only driving force is surface tension. The numerical results for different initial shapes appear to be circular to the eye, which are obtained for $t = 10$.

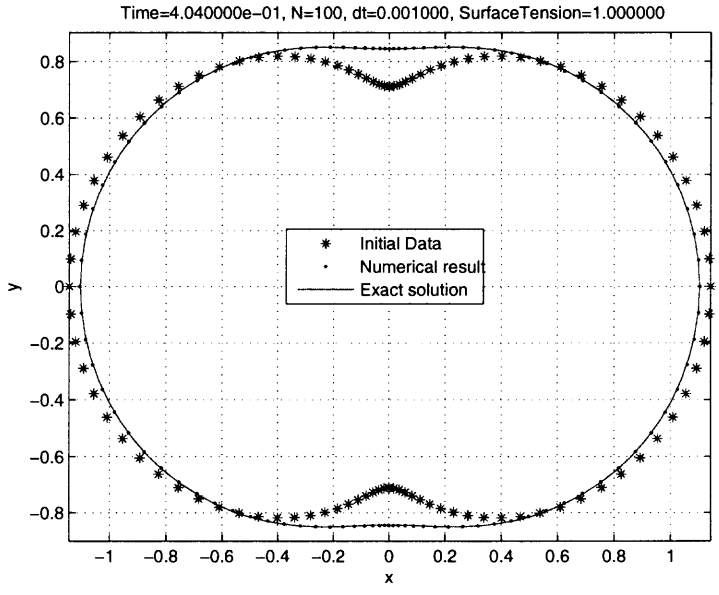


**Figure 3.3** Comparison with the exact solution.

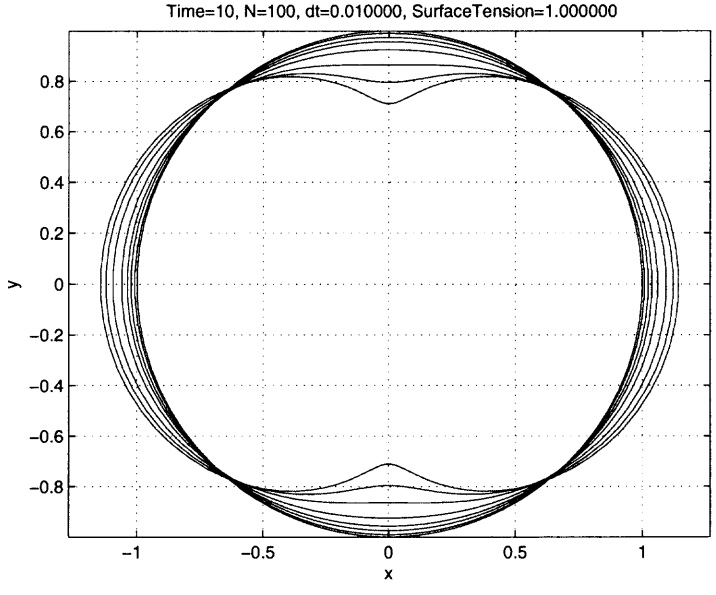


**Figure 3.4** Evolution of a nephroid. T1=0.2, T2=.05, T3=1, T4=1.5, T5=2, and T6=10.

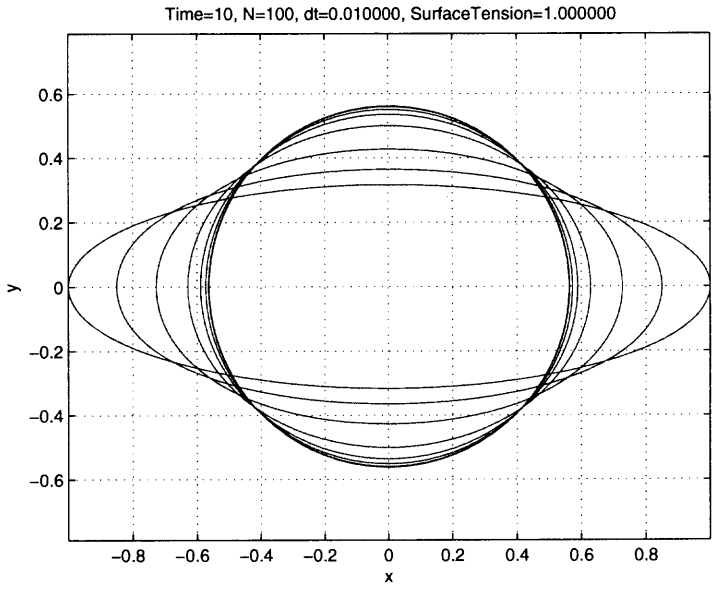


**Figure 3.5** Evolution of an ellipse. T1=0.2, T2=.05, T3=1, T4=1.5, T5=2, and T6=10.

In these numerical calculations, we do not use symmetric properties of the flow directly, i.e., the velocity field is calculated for the entire free surface. However there is a difficulty that the matrix (3.4) is close to singular. The reason is the existence of a zero eigenvalue for the system of equations (3.36), (3.37), (3.47) and (3.48), which seems to be due to the nonuniqueness of the stream function. The difficulty is resolved by assuming the stream function where the interface intersects the $x$-axis (which is a streamline for the flow) is 0, which means we impose one stream function value in our calculation. The curvature is evaluated by $\frac{d\theta}{ds}$, where $\theta$ is the tangential angle and $s$ is the arc length (see Appendix A).

The second test problem is the flow of a viscous fluid in a corner. A similarity solution describing the flow between a planar solid surface and a planar free surface was derived by [41]. In order to numerically compute the solution for the Moffatt flow, we truncate the geometry as shown in Figure 3.6 where the no-slip interface extends from $s = 0$ to 1 and the free surface from $s = 1$ to 2 and an arc of a circle

is used to smoothly connect the sides of the corner. We impose the analytic values of the stream function and its derivative according to the theoretical solution at the arc of the circle. Figure 3.7 shows $\Psi$, $\frac{\partial \Psi}{\partial n}$, $\omega$ and $\frac{\partial \omega}{\partial n}$ versus arclength $s$ for the exact and computed solution.The corner is at $s = 1$. As shown in the figure, the numerical solution matches the exact solution very well: the solid line is the exact solution and the symbol "+" is the computational solution. The advantage of this calculation is that vorticity $\omega$ and its derivative $\omega_n$ are well described by this numerical calculation even if their values are divergent at the corner.

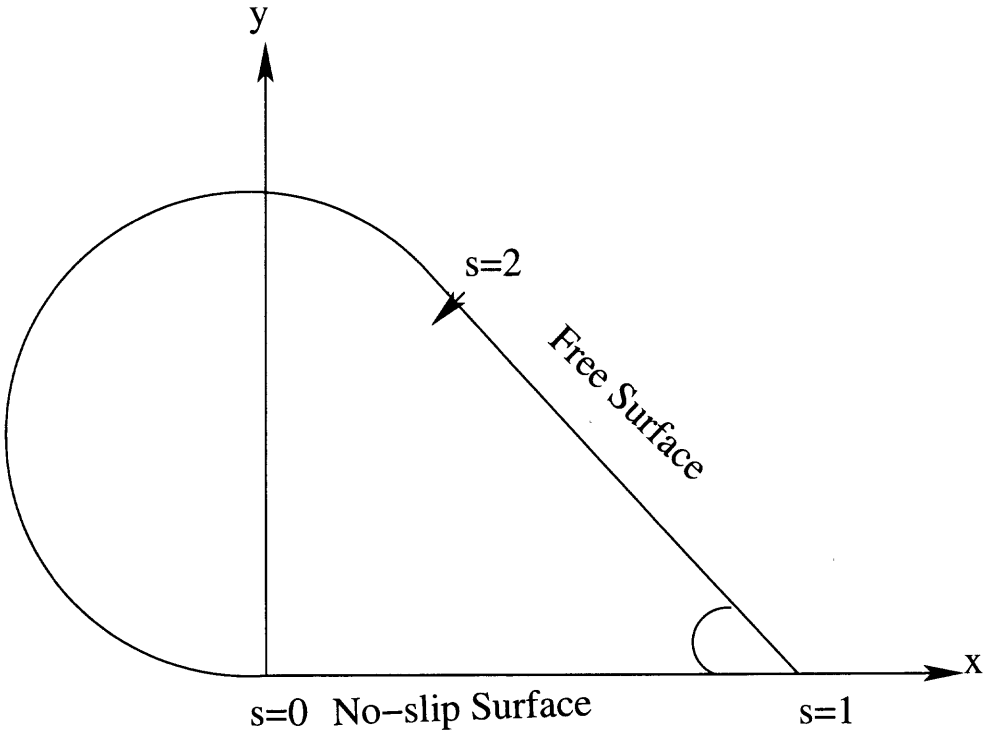


**Figure 3.6** Geometry of the flow in a corner. The angle of the corner is $\alpha = 1$.

In Figure 3.8, we use the methods described above to simulate a drop spreading without surface tension on a horizontal plane. The initial shape is part of a circle. During the calculation, the time step is adaptive in order to make sure that the point above the substrate touches the substrate exactly. Since the only force is gravity, the drop will spread forever. Here the final time is $t = 32$. If we want to go further, more

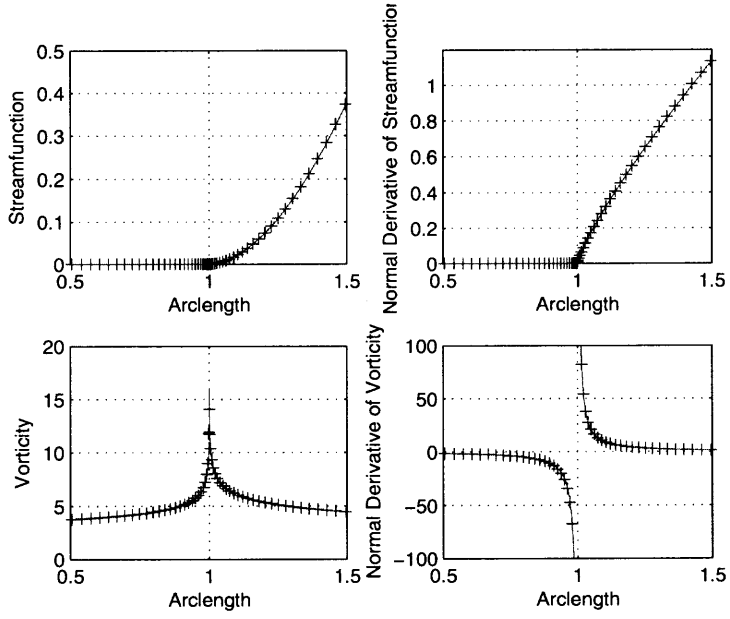


**Figure 3.7** Comparison with the exact solution of the flow in a corner.The solid line is the exact solution. The symbol "+" is the computational solution.

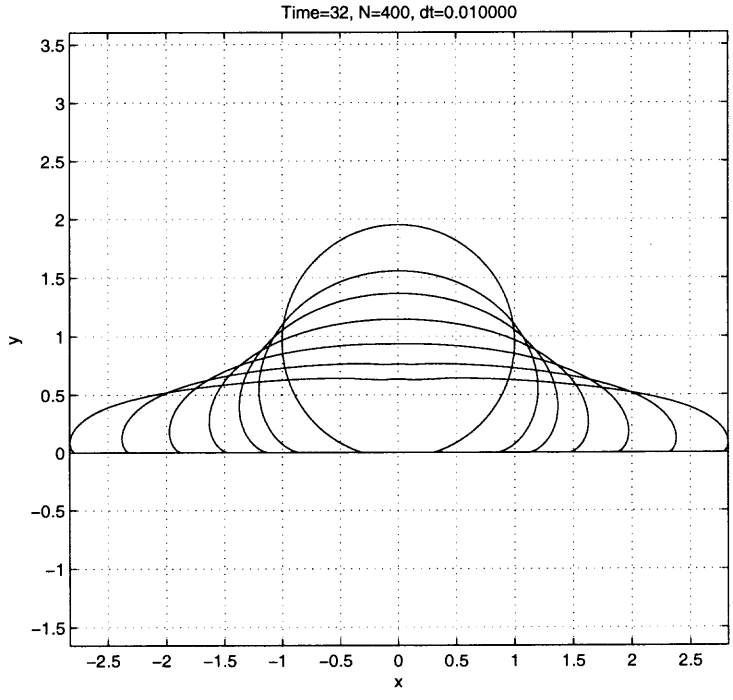


**Figure 3.8** The drop spreading driven by gravity without surface tension.T=0, T=1, T=2, T=4, T=8, T=16, and T=32.

points are need to describe the contact region better. Here the contact angle is not specified which is different from what we do for rolling droplets. When we calculate the rolling motion, the contact angle is fixed at $180^0$.

The third test is to use the code to calculate the velocity field of a steady drop. A viscous drop is assumed to stick to an inclined plane without motion. Since the velocity of the drop is zero, the Stokes equation becomes

$$\frac{\partial p}{\partial x} = \rho g \sin\alpha, \tag{3.50}$$

$$\frac{\partial p}{\partial y} = \rho g \cos\alpha, \tag{3.51}$$

where $p(x, y)$ is pressure inside the drop, $\rho$ is fluid density, $g$ is acceleration of the gravity, and $\alpha$ is a tilt angle. The tangential stress balance is automatically satisfied. The normal stress balance is,

$$p = \sigma \frac{d\theta}{ds}, \tag{3.52}$$

where $\sigma$ is surface tension, $\theta$ is the tangent angle on the interface, and $s$ is the arc length along the interface moving in the counterclockwise direction. The pressure outside the drop is assumed to be zero. Integrating the equations (3.50) and (3.51), we obtain

$$p = \rho g(x \sin\alpha - y \cos\alpha) + p_c, \tag{3.53}$$

where $p_c$ is the hydrostatic pressure. Substituting the equation (3.53) of pressure into the normal stress balance equation (3.52), we obtain

$$\rho g(x \sin\alpha - y \cos\alpha) + p_c = \sigma \frac{d\theta}{ds}. \tag{3.54}$$

The equation (3.54) is solved numerically to obtain the shape of the motionless drop. This steady shape will then be used as initial data in the boundary element calculation to verify that this shape gives an approximate motionless solution to the

discrete boundary element equations. Since this is a first order ordinary differential equation, we can not specify both the advancing contact angle and the receding contact angle. Here we specify the advancing contact angle and integrate the equation (3.54) along the interface to get the interface shape and receding contact angle. After the steady shape is obtained, we use boundary element method to calculate the velocity field on the interface to update the interface. In Figure 3.9, the star is the initial shape and the circle is the shape at $t = 2$. This numerical simulation shows that the drop moves very slowly. This means our code is able to describe the velocity field of the interface.

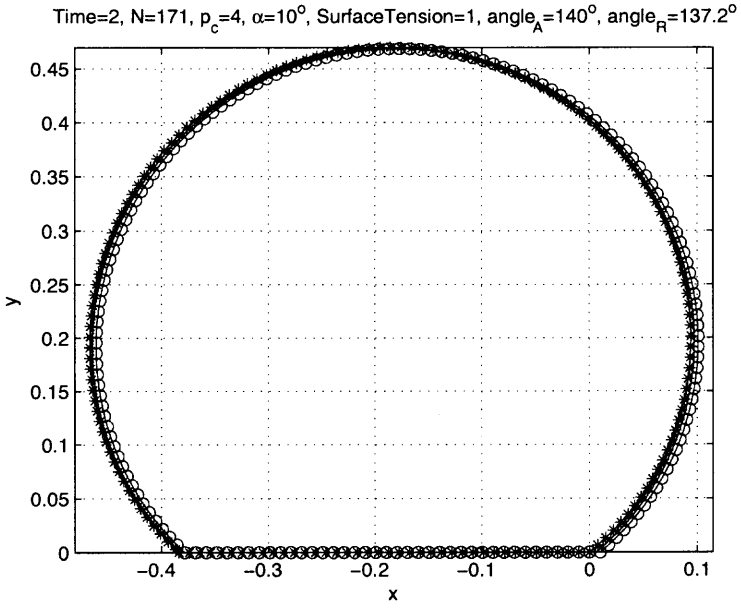


**Figure 3.9** The calculation by the boundary element method shows that the steady drop moves very slowly (velocities about $10^{-3}$). $*$ is the initial shape and $o$ is the shape at $t = 2$.

## 3.6 Rolling Droplets

As noted before, there is a singularity at the contact line when the usual hydrodynamic assumptions are applied. However the contact angle $\pi$ is considered as a special case (called rolling motion) in which the singularity is absent. The local analysis

in [11, 24] showed that the singularity is removed for the rolling motion without a hydrostatic pressure term. However there is a sign error in their analysis pointed out by Dussan [7]. Mahadevan and Pomeau [25] considered the leading order pressure as $r \to 0$ to be the constant hydrostatic pressure and derived the shape of the free surface $y(x)$ from the normal stress balance equation and the stream function $\Psi$ in the vicinity of the contact point:

$$y = \frac{x^2}{2R} \tag{3.55}$$

$$\Psi = -\frac{r^2 U}{2R}(1 - \frac{\theta}{\pi} + \frac{\sin 2\theta}{2\pi}) \tag{3.56}$$

where $U$ is the characteristic velocity, R is the characteristic length, and $r$ and $\theta$ are as in Figure 3.10. These results are based on sufficiently small radius $r$, the capillary number $Ca = \frac{\mu U}{\sigma}$ and the Bond number $Bo = \frac{\rho g R^2}{\sigma}$. Unfortunately they overlooked a balance in the Stokes equation. The stream function they derived satisfies the biharmonic equation, but it does not satisfy the Stokes equation if the leading order pressure is taken to be constant. The details of this local analysis are given in chapter 4.

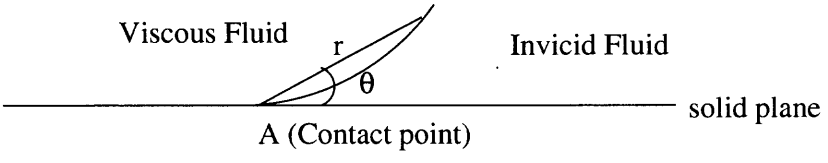


**Figure 3.10** The immediate vicinity of the contact point.

All these local analysis and experiments [36] motivate us to consider a rolling drop with a contact angle of $180^0$ as a simple model for the motion of viscous drops on an inclined non-wettable plane. Numerically the local shape in the vicinity of the contact line is considered as a parabola. This is a reasonable choice, in view of the simplicity of enforcing this condition and its consistency with the lubrication

approximation (see details in Chapter 4). We will show how this local shape affects the numerical calculation.

Consider first a droplet spreads under the influence of gravity and surface tension on a flat non-wettable plane. Figure 3.11 shows that the droplet reaches a steady shape due to the balance of the gravity and capillary force. The numerical results for time $T = 4, T = 8$ and $T = 16$ are already overlapped, which means velocities of the drop at these time are small (about $10^{-3}$). Thus we can consider that the drop is at the steady state. As a check on the numerics, Figure 3.12 shows the volume conservation during the process. Here the maximum volume change is about 0.22%.

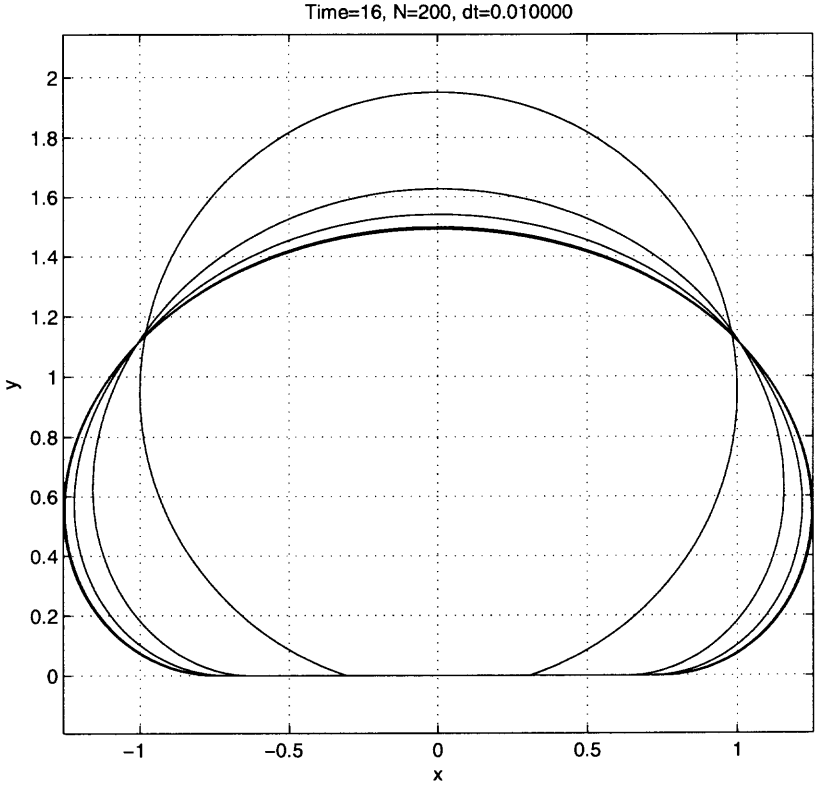


**Figure 3.11** The steady state solution for drop spreading with gravity and surface tension. T=0, T=1, T=2, T=4, T=8, and T=16.

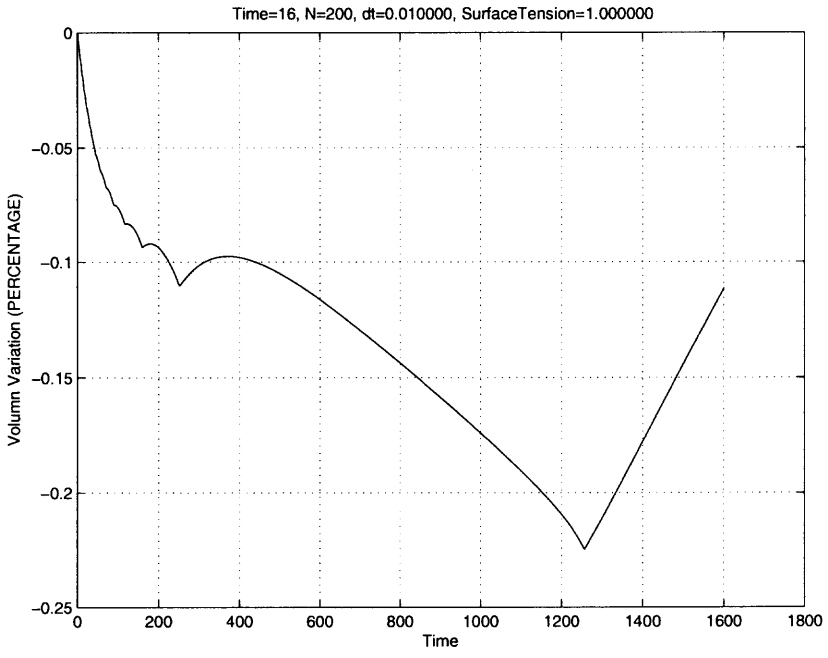


**Figure 3.12** Volume conservation for a spreading drop.

Next we consider a droplet moving on an inclined plane. In the numerical simulation, a parabola is used to move the front and back contact lines through the last tow grid points (See Figure 3.13). In Figure 3.13, the coordinates of $p_1$, $p_2$ and $p_3$

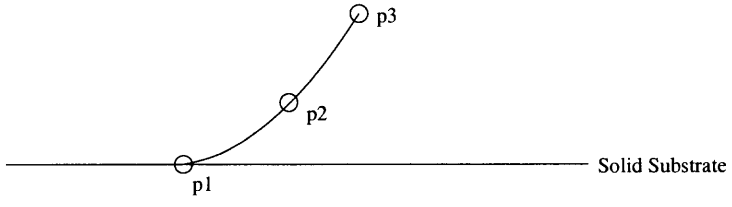


**Figure 3.13** Move the contact line by a parabola through the last two grid points.

are $(x_1, 0)$, $(x_2, y_2)$ and $(x_3, y_3)$ respectively. These three grid points satisfy a parabola

$$y = A(x - x_1)^2, \tag{3.57}$$

where $A$ and $x_1$ are unknowns which are determined by points $p_2$ and $p_3$. The first derivative at $p_1$ is zero $y'(x_1) = 0$ at the contact line which means the free surface of the drop is tangent to the solid substrate so that the contact angle is $\pi$. Since points

$p_2$ and $p_3$ satisfy the equation of the parabola as well, then

$$\begin{aligned} y_2 &= A(x_2 - x_1)^2, \\ y_3 &= A(x_3 - x_1)^2. \end{aligned} \tag{3.58}$$

Solve $A$ and $x_1$ from the equations (3.58),

$$x_1 = \frac{x_2\sqrt{y_3} - x_3\sqrt{y_2}}{\sqrt{y_3} - \sqrt{y_2}}, \tag{3.59a}$$

$$A = \left(\frac{\sqrt{y_3} - \sqrt{y_2}}{x_3 - x_2}\right)^2. \tag{3.59b}$$

The boundary element method introduced before is used to update the free surface. A parabola is used to approximate the shape of free surface in the contact region so that the contact points can be moved. Every time step, cubic splines are used to redistribute grid points in order to make the arc length of the boundary elements nearly equal. In order to keep the consistency, the assumption of a $180^0$ contact angle is used in the cubic spline. The plot of velocity field in Figure 3.14 shows that the droplet does roll on an inclined plane instead of sliding.

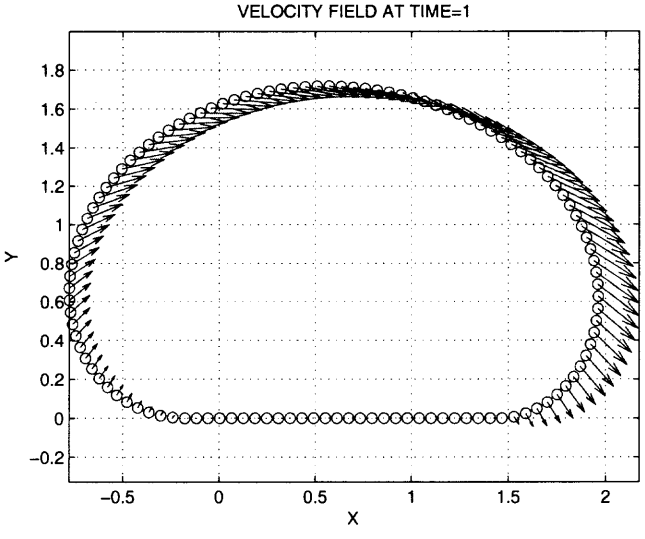


**Figure 3.14** Velocity field of a droplet moving on an inclined plane at $T = 1$.

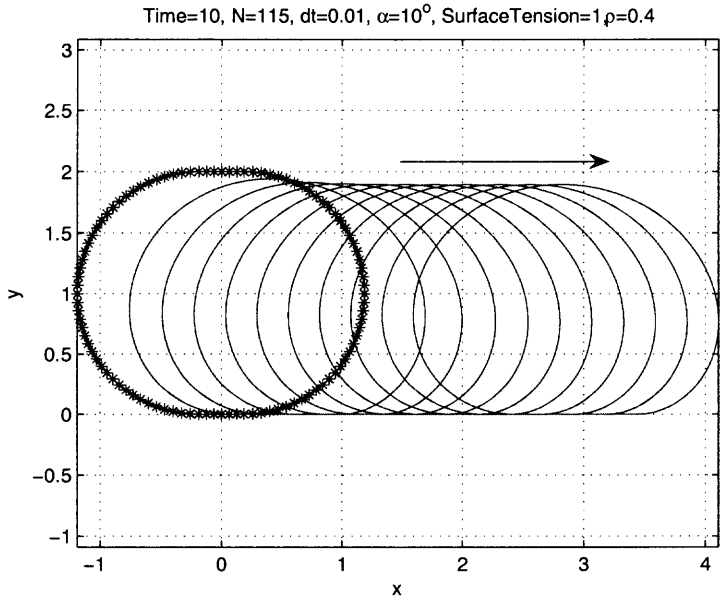


**Figure 3.15** A light droplet with $\rho = 0.4$ rolls on an inclined plane. Finally it reaches a steady state. Time $= 0, 1, 2, 3, 4, 5, 6, 7, 8, 9, 10$.

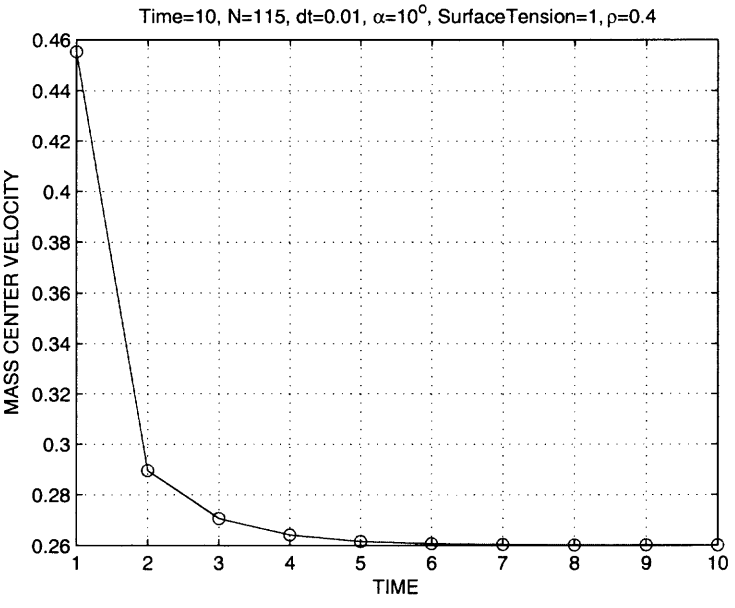


**Figure 3.16** A light droplet with $\rho = 0.4$ reaches a steady velocity.

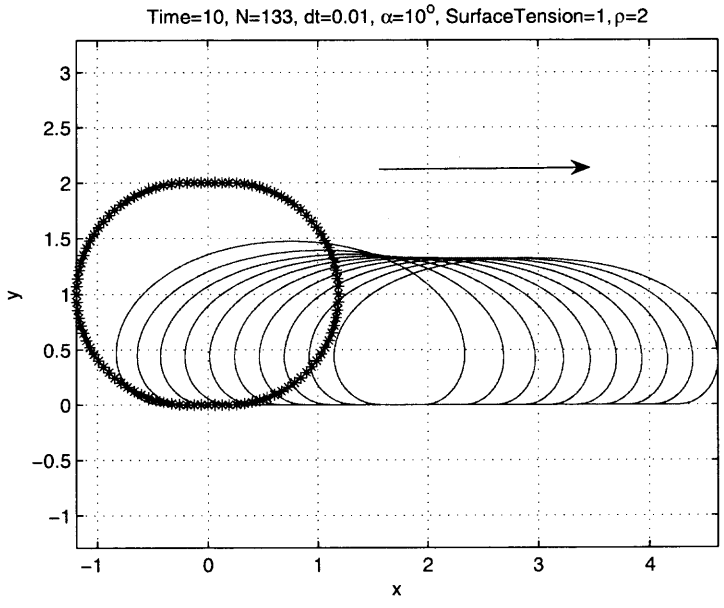


**Figure 3.17** A heavy droplet with $\rho = 2$ rolls on the inclined plane. Finally it reaches a steady state. Time $= 0, 1, 2, 3, 4, 5, 6, 7, 8, 9, 10$.

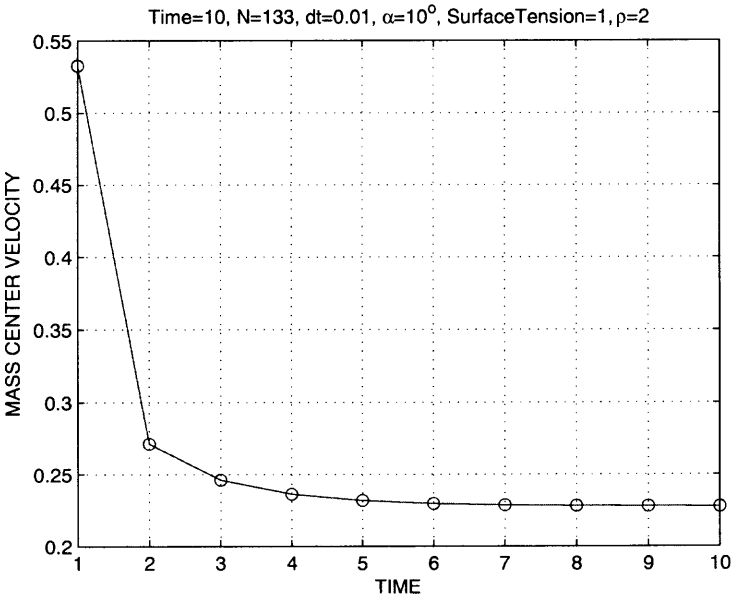


**Figure 3.18** A heavy droplet with $\rho = 2$ reaches a steady velocity.

There are several interesting phenomena about this rolling drop. A rolling drop goes to a steady velocity which is determined by the balance between the gravitational potential energy which accelerates it and the viscous energy dissipation which retards it. A steady state is reached when these two forces are balanced. The Figure 3.17 shows that a light drop with $\rho = 0.4$ reaches a steady velocity about 0.26. The Figure 3.18 shows that a heavy drop with $\rho = 2$ reaches a steady velocity about 0.23. A drop is called "light" or "small" when the radius of drop is less than the capillary length $(\frac{\sigma}{\rho g})^{1/2} = 1.58$ when the values of parameters are $\sigma = 1$, $g = 1$ and $\rho = 0.4$. On the other hand, a drop is called "heavy" or "large" when the radius of drop is greater than the capillary length $(\frac{\sigma}{\rho g})^{1/2} = 0.71$ when the values of parameters are $\sigma = 1$, $g = 1$ and $\rho = 2$. In these numerical calculations, the tilt angle $\alpha = 10^0$.

In Figure 3.16 and 3.18, the velocities are evaluated in such a way that

$$V_{i+1} = \frac{X_{i+1} - X_i}{t_{i+1} - t_i}, \tag{3.60}$$

where $V_{i+1}$ denotes the velocity at time $t_{i+1}$ and $X_i$ denotes the $x$ coordinates at time $t_i$. Here the time period $t_{i+1} - t_i$ is not the time step that we use in numerical calculation. We mostly use $t_{i+1} - t_i = 1$. Although this can not accurately describe the velocities at the beginning, it can describe the velocities well as the drop goes to a steady state.

Mohadevan and Pomeau [25] use a simple scaling theory to predict the steady velocity of drops rolling down an inclined plane under the influence of gravity and surface tension. They obtained a counter-intuitive result that steady velocity decreases as the radius increases for sufficiently small size droplets. When the drop size is less than the capillary length $(\sigma/\rho g)^{1/2}$, the drop is almost a sphere because the surface tension is dominant. Therefore the drop rolls like an elastic ball from the exterior. Applying this theory to the $2D$ drops, we have that the steady velocity for sufficiently

small droplets scales as

$$U \sim \frac{\sigma^2 \sin\alpha}{\mu\rho g R^2} = \frac{\sigma \sin\alpha}{\mathrm{Bo}\mu}, \tag{3.61}$$

where $\mathrm{Bo} = \frac{\rho g R^2}{\sigma}$ is the Bond number, and $\alpha$ is the tilt angle of the plane. The result is surprising because the steady velocity of small droplets is inversely proportional to the drop size even though the driving force of gravitation grows very fast, which is the order of $R^3$ in $3D$ ( $R^2$ in $2D$). But in fact, the viscous force grows faster than the gravitational force. The reason is that the contact region increases rapidly because of the growth of gravitational force.

Their theory also predicts that when the radius of the droplet is much larger than the capillary length $(\sigma/\rho g)^{1/2}$, the steady velocity does not depend on the size of the drop. In other words, the velocity does not depend on liquid density and acceleration of gravity either. These results are similar to the results of a $3D$ droplet derived by Mahadevan and Pomeau [25]. Specialized to $2D$, the result of Mahadevan and Pomeau (correcting for some errors in their paper) states that the velocity of sufficiently large drops scales as

$$U \sim \frac{\sigma}{\mu} \sin\alpha. \tag{3.62}$$

A different argument which leads to (3.62) but does not depend on dimension is given later in this section.

Since the analysis leading to equations (3.61) and (3.62) is only a rough scaling analysis, we have performed numerical computations in an attempt to verify the scaling relations. Instead of changing the size of the droplet, we vary the density of droplet so that we can have same number of nodes on the boundary for different droplets. This can equivalently show that the steady velocity of large droplets does not depend on the drop size. Otherwise, changing the radius of droplets may cause some numerical error because of different size and number of boundary elements. The

results of the computation are shown in Figure 3.19. The horizontal axis is the density $\rho$ varying from 0.2 to 2. The vertical axis is the steady velocity. In this calculation, other parameters are $\sigma = 1$, $\mu = 1$ and $g = 1$. In Figure 3.19, it shows that the velocity decreases as the density increases for small density, while velocity goes to a constant as the density goes to a large value.

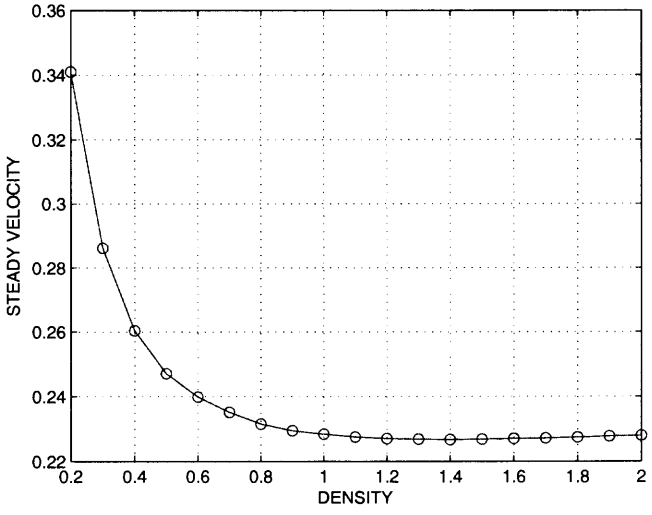


**Figure 3.19** The steady velocity of the rolling drop for the different liquid density.

For a large or heavy droplet (called a pancake), Richard and Quere [8] theoretically gave a more precise result of the steady velocity. It is well known that the contact angle $\theta$ is determined by the Young relation

$$\sigma_S = \sigma_{SL} + \sigma \cos\theta, \tag{3.63}$$

where $\sigma_S$, $\sigma_{SL}$ and $\sigma$ are the solid/air, solid/liquid and liquid/air interface tension respectively. If the droplet sits on a hydrophilic solid (which likes water), the droplet will spread out completely and the contact angle will be very small (close to 0). On the other hand, if the droplet sits on a super-hydrophobic solid (which does not like water), the contact angle $\theta$ will be very large (close to $180^0$). Roughly speaking, the surface tension of a solid $\sigma_S$ is very small because the solid is hydrophobic.

The roughness of the super-hydrophobic solid makes air be trapped between liquid and solid. The solid/liquid interface is almost like the liquid/air interface. Thus the interface tension of solid/liquid is approximately equal to the surface tension of liquid/air $\sigma_{SL} = \sigma$, then $\cos\theta = -1$. This is the reason that the roughness of the

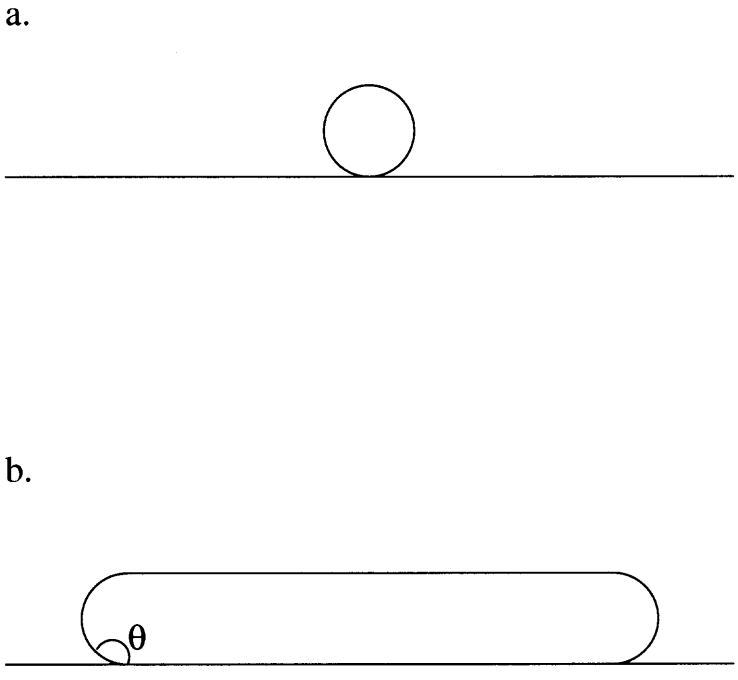


**Figure 3.20** Equilibrium shape of droplets on the super-hydrophobic surface: (a) a droplet in capillary regime; (b) a droplet in gravity regime. $\theta$ is the contact angle.

super-hydrophobic solid leads to a very large contact angle $180^0$. The equilibrium shapes of a droplet are shown in Figure 3.20. If the drop is small, the capillary force is dominant and the gravity is negligible. Therefore the pressure in the droplet is uniform and the shape is almost a sphere. If the drop is large, the gravity is important and is not negligible. The droplet is flattened by gravity and forms a "pancake". The hydrostatic pressure inside the droplet is equal to $\rho gh$ where $\rho$ is the liquid density, g is acceleration of gravity, and $h$ is the depth from the free surface. If the thickness is $h_0$, the equation of the balance in horizontal forces is

$$\sigma_S + \frac{1}{2}\rho g h_0^2 = \sigma_{SL} + \sigma. \tag{3.64}$$

Combine the equation (3.63) and the equation (3.64), and solve the thickness [12]

$$h_0 = \sqrt{\frac{2(1-\cos\theta)\sigma}{\rho g}}. \tag{3.65}$$

The viscous force in the large rolling drop is approximated by that in the liquid layer flowing down an inclined plane (see Figure 3.21). The viscous force per unit volume is $\mu\frac{\partial^2 u}{\partial^2 y} = p_x$ according to Poiseuille law. Two boundary conditions are the no-slip boundary condition at the plane $u(0) = 0$ and no shear at the free surface $\frac{\partial u(0)}{\partial y} = 0$. Then the velocity is

$$u = \frac{1}{\sigma}p_x(\frac{y^2}{2} - h_0 y) \tag{3.66}$$

The average velocity is

$$V_0 = \frac{1}{h_0}\int_0^{h_0} dy. \tag{3.67}$$

This yields the viscous force

$$\frac{3\sigma V_0}{h_0^2}. \tag{3.68}$$

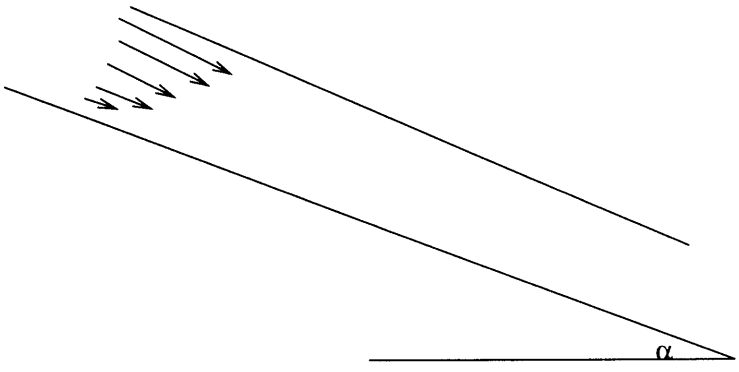


**Figure 3.21** Liquid layer falls down an inclined plane.

In the steady flow, the shear stress is balanced by the gravity

$$\frac{3\sigma V_0}{h_0^2} = \rho g \sin\alpha, \tag{3.69}$$

where $\alpha$ is the tilt angle. Substituting for $h_0$ in equation 3.65, we obtain the equation

$$3\sigma V_0 = 2\sigma(1 - \cos\theta)\sin\alpha. \tag{3.70}$$

Thus the steady velocity of a pancake rolling down an inclined plane is [8]:

$$V_0 = \frac{2(1 - \cos\theta)}{3}\frac{\sigma}{\mu}\sin\alpha, \tag{3.71}$$

In the numerical calculation shown in Figure 3.19, the values of parameters are $\theta = 180^0$, $\sigma = 1$, $\mu = 1$ and $\alpha = 10^o$ respectively. According to the theoretical prediction, the value of the steady velocity in the equation (3.71) is about 0.2315. On the other hand, the numerical calculation shown in Figure 3.19 shows that the steady velocity goes to about 0.23 as the drop size becomes very large which has a very good agreement with the theoretical prediction.

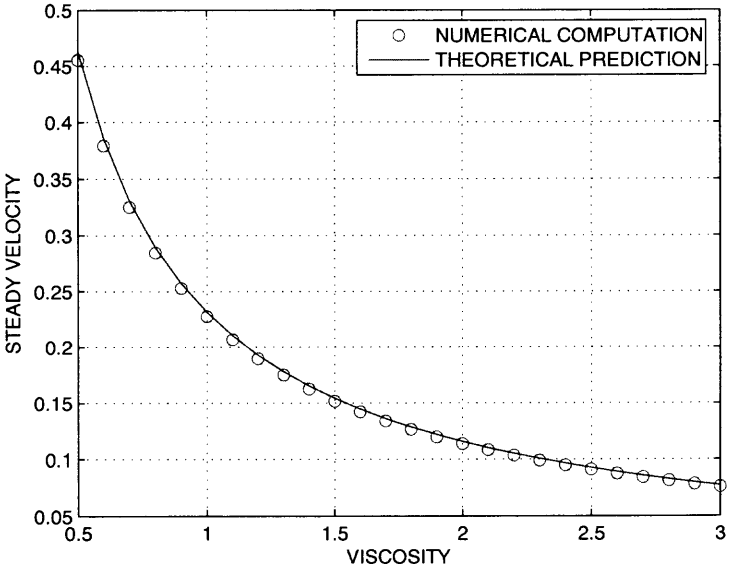


**Figure 3.22** Comparison of the theoretical steady velocity to numerical results for different liquid viscosity.

The Figure 3.22 shows how the steady velocity depends on the liquid viscosity for the large droplet. The values of parameters we used in the calculation are the

contact angle $\theta = 180^0$, surface tension $\sigma = 1$, the tilt angle $\alpha = 10^0$ and density $\rho = 2$ respectively. The liquid viscosity varies from 0.5 to 3. Here the droplet is large enough ($\rho = 2$) for this set of parameters because the radius of droplet in the numerical calculation is greater than 1 while the capillary length is $\sqrt{\frac{\sigma}{\rho g}} = 0.7$. In the figure 3.22, the solid line is theoretical calculation using the formula (3.71), and the circles represent the numerical calculation. First the numerical result shows that the steady velocity decreases as the viscosity increases. This is because energy dissipates more when the friction inside the fluid is stronger due to larger viscosity. More precisely, the steady velocity of large droplets is inversely proportional to liquid viscosity. It matches the theoretical prediction very well.

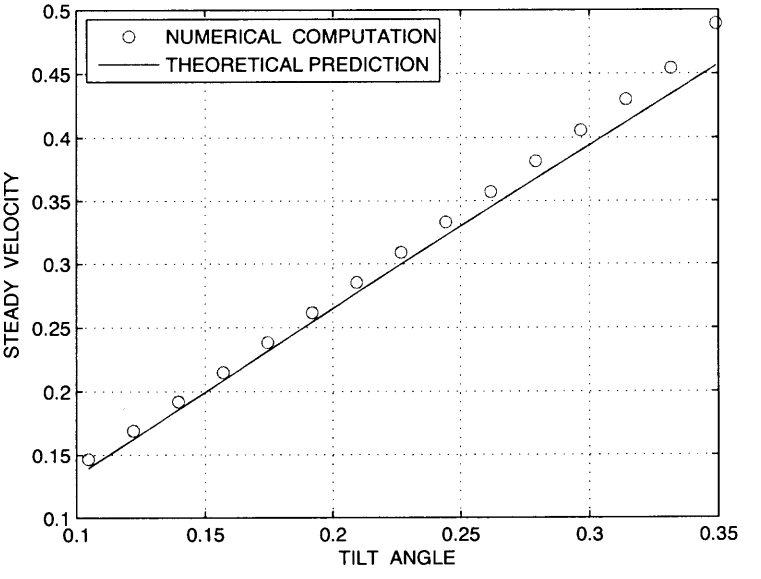


**Figure 3.23** Comparison of the theoretical steady velocity to numerical results for different tilt angles. The angle is measured in radians.

The Figure 3.23 shows how the steady velocity depends on the tilt angle for the large droplet with $\rho = 2$ and all other parameters are 1. The tilt angle varies from $6^o$ to $20^o$ which is measured in radians in the figure. The solid line represents the theoretical prediction which is a sine function. The circles represent the numerical

result. It shows the numerical result matches well the theoretical prediction when the tilt angle is not very large. The difference between the numerical result and the theoretical prediction becomes slightly larger when the tilt angle becomes larger. A likely reason is that for larger tilt angles the drop is less flattened, (i.e., less 'pancake like').

## 3.7 Numerical Analysis

The parabolic interface shape is imposed only over a few mesh points, and hence a small region near the contact line. Our numerical calculation cannot distinguish a significant difference on the global shape and dynamics in using

$$y = A(x - x_0)^q \tag{3.72}$$

for shape near the contact line $x = x_0$ for $p$ near 2. However, the calculation does distinguish a difference in using a $180^0$ contact angle (i.e., a shape of (3.72)) and a corner (i.e., the contact angle is less than $180^0$) and that is crucial.

As we mentioned in the previous section, there is a stress singularity at the contact line when we assume a Newtonian fluid with the no-slip condition on the solid surface and the contact angle is less than $180^0$. In the numerical calculation, this singularity at the contact line can be avoided by calculating all values at the mid points instead of at the nodes [30]. This gives an effective numerical regularization of the stress singularity. As shown by Moriarty and Schwartz [19], there is always some amount of numerical slip in this calculation since the no-slip condition can only be enforced at discrete nodes, but the no-slip condition is not enforced in the vicinity of the contact line. Moriarty and Schwartz [19] showed that this kind of numerical slip is equivalent to the slip model (e.g. Navier-type) in a small region local to the contact line. Homsy and his coworkers [1] used the above idea to show that the numerical solution does not converge as the grid-spacing goes to zero, instead

diverging logarithmically. They found that the maximum height of the free surface profile increases linearly as the logarithm of the mesh size decreases.

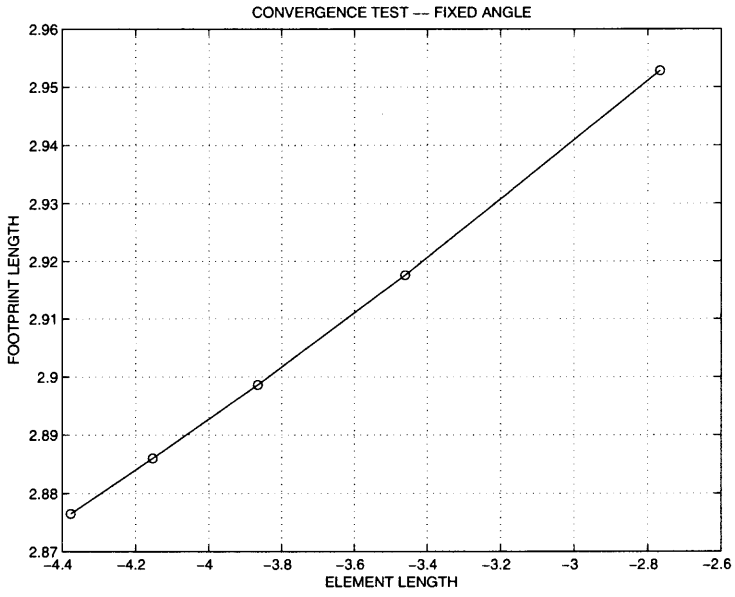


**Figure 3.24** The footprint decreases linearly as the logarithm of the mesh size decreases for the rolling drop with the contact angle being $120^o$.

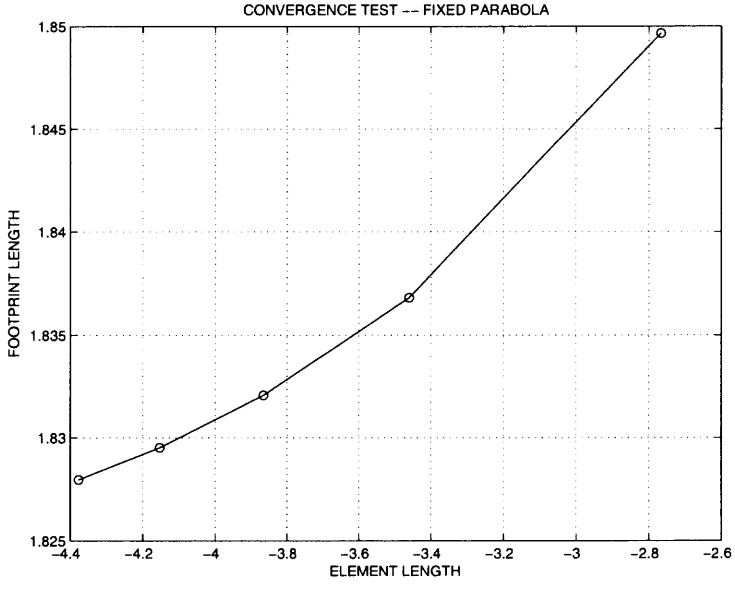


**Figure 3.25** The footprint approaches slowly to a constant as the logarithm of the mesh size decreases for the rolling drop with the contact angle being $180^0$.

We use the footprint which is the length of contact region as the characteristic parameter instead of the height of the profile used by other paper [1] to get similar divergence results as the grid-spacing goes to zero. This means the numerical calculation diverges when the grid-spacing is refined. The Figure 3.24 shows that the footprint of the drop plotted versus logarithm of the length of the element in the contact region. The figure indicates that the footprint decreases linearly as the logarithm of the mesh size decreases for the rolling drop with the contact angle being $120^o$. The lack of convergence of the numerically calculated shape as the number of gridpoints increases is consistent with the notion that there is a stress singularity at the contact point. In other words, this divergence property will disappear if the singularity is absent. As we mentioned before, there does not exist this stress singularity with the contact angle being $\pi$. In Figure 3.25, the footprint approaches slowly to a constant as the logarithm of the mesh size decreases for the rolling drop with the contact angle being $\pi$, which suggests there is no stress singularity at the contact line for the rolling motion.

In the case when the contact angle is less than $\pi$, so that there is a corner at the contact point, we evolve the location of the contact point in a manner similar to [23]. The parabolic equation

$$x = ay^2 + by + c, \tag{3.73}$$

is used to move the contact line. In this equation (3.73), the coefficients $a$, $b$, and $c$ are unknowns that are determined by the last two grid points and the contact angle. We assume the contact angle is fixed during the motion.

In Figure 3.26, the last two grid points $p_2(x_2, y_2)$ and $p_3(x_3, y_3)$ and the contact angle $(\pi - \zeta)$ are known. The contact line $p_1(x_1, 0)$ needs to be determined. All these

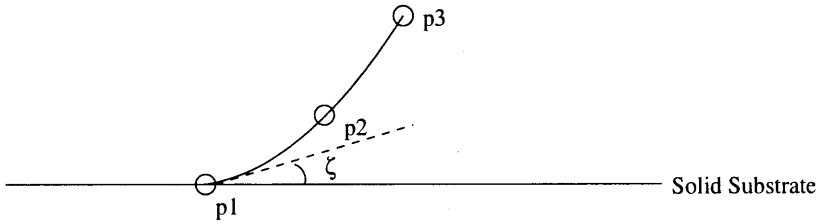


**Figure 3.26** Move the contact line by a parabola.

three grid points are assumed to be on the same parabolic equation (3.73),

$$\begin{aligned} x_2 &= ay_2^2 + by_2 + c, \\ x_3 &= ay_3^2 + by_3 + c, \\ \frac{dx}{dy}|_{(x_1,0)} &= \frac{1}{\tan\zeta}. \end{aligned} \tag{3.74}$$

It is obvious $x_1 = c$. Thus the contact line $x_1$ is

$$x_1 = \frac{x_3y_2^2 - x_2y_3^2 - (y_3y_2^2 - y_2y_3^2)/\tan\zeta}{y_2^2 - y_3^2}. \tag{3.75}$$

## 3.8 Rolling Droplets with Surfactant

Spreading control of droplets is very important in engineering applications such as printing and microfluidics. For capillary-related applications, it is quite difficult to control the spreading and motion of droplets on surfaces. Chemical treatment is a common way used to tune the wetting and spreading behavior. Recently there has been much interest in using the influence of surfactant adsorption to turn superhydrophobic surfaces into highly wettable surfaces, this is becoming a new and attractive research field [13, 35, 44]. Paper [35] found that superhydrophobic surfaces remain in superhydrophobic range for most common surfactants and contact angles do not decrease significantly on superhydrophobic surfaces. Our work is focused on the influence of surfactant on the dynamics of rolling motion rather than its effect on the contact angle. Although our model allows surfactant transport to and from the

substrate to take place [10], in the simulations presented here, we assume there is no surfactant coming or going from the solid for the simplicity.

The governing equations are Stokes equations which are written in the integral form (Equation 3.15 and 3.16). For the simplicity, we use the linear relation between surfactant concentration and surface tension

$$\sigma = \sigma_0(1 - \beta\frac{\Gamma}{\Gamma_0}), \tag{3.76}$$

where $\sigma_0$ is the surface tension of a clean surface, $\Gamma_0$ is the initial surfactant concentration, and the parameter $\beta$ will be referred to as the sensitivity parameter. The normal stress balance (NSB) in the terms of the stream function is

$$\frac{\partial\omega}{\partial n} + 2\frac{\partial^2}{\partial s^2}(\frac{\partial\Psi}{\partial n}) - 2\frac{\partial}{\partial s}(\kappa\frac{\partial\Psi}{\partial s}) = -\frac{1}{\mu}\frac{\partial\sigma}{\partial t}\kappa - \frac{\sigma}{\mu}\frac{\partial\kappa}{\partial t} + \frac{\rho g}{\mu}(t_x\sin\alpha - t_y\cos\alpha), \tag{3.77}$$

and the tangential stress balance (TSB) in the terms of the stream function is

$$-\omega + 2\frac{\partial^2\Psi}{\partial s^2} + 2\kappa\frac{\partial\Psi}{\partial n} = \frac{1}{\mu}\frac{\partial\sigma}{\partial t}. \tag{3.78}$$

The boundary condition at the solid is as before – the no-slip boundary condition,

$$\Psi = 0, \tag{3.79}$$

and

$$\frac{\partial\Psi}{\partial n} = 0. \tag{3.80}$$

The finite-volume method [22, 31] is used to track the evolution of insoluble surfactant on the surface. The evolution of surfactant concentration at the surface is governed by an advection-diffusion equation [17]. The two-dimension case is

$$\left.\frac{\partial\Gamma}{\partial t}\right|_n + \frac{\partial}{\partial s}(u_s\Gamma) + \Gamma\kappa u_n = \frac{1}{Pe}\frac{\partial^2\Gamma}{\partial s^2}, \tag{3.81}$$

where the Peclet number $Pe = \frac{UL}{D_s}$ and the time derivative is in fixed normal coordinates. We integrate this equation in two steps. First we solve

$$\left.\frac{\partial \Gamma}{\partial t}\right|_n + \frac{\partial}{\partial s}(u_s \Gamma) = \frac{1}{Pe}\frac{\partial^2 \Gamma}{\partial s^2}, \tag{3.82}$$

which gives the changes in surfactant due to advective and diffusive flux. The corresponding difference equation is

$$\frac{(\Gamma_i^{n+1} - \Gamma_i^n)\Delta s_i^n}{\Delta t} + (u_s\Gamma)_{i+1/2}^n - (u_s\Gamma)_{i-1/2}^n = \frac{1}{Pe}\left(\left(\frac{\partial \Gamma}{\partial s}\right)_{i+1/2}^n - \left(\frac{\partial \Gamma}{\partial s}\right)_{i-1/2}^n\right). \tag{3.83}$$

Second, we integrate

$$\left.\frac{\partial \Gamma}{\partial t}\right|_n + \Gamma \kappa u_n = 0, \tag{3.84}$$

which gives the change in surfactant due to stretcher at the interface. During this step, the total amount of surfactant is conserved within each boundary element, since the interface markers move with the local fluid velocity. The new surfactant concentration is evaluated in the second step as

$$\Gamma_i^{n+1} = \frac{\Gamma_i^n \Delta s_i^n}{\Delta s_i^{n+1}}. \tag{3.85}$$

The Figure 3.27 shows that a drop with surfactant rolls down an inclined plane (density $\rho = 1$, sensitivity $\beta = 0.4$, tilt angle $\alpha = 10^o$ and Peclet number $Pe = 100$). In order to clearly observe the effect of surfactant and reduce the impact of larger velocity at the beginning on surfactant transport at the contact line, the droplet runs without surfactant from $T = 0$ to $T = 6$. The insoluble surfactant is present at the surface from $T = 6$. The drop goes to another steady velocity. The Figure 3.28 shows the rolling drop reaches a steady velocity with and without surfactant. The Figure 3.29 is about the distribution of surfactant on the surface. The amount of surfactant at the advancing contact line is about ten times of the amount of surfactant at the receding contact line. The Figure 3.30 is the plot of the curvature at nodes of free

surface. At the advancing contact line, the curvature is not completely smooth. It may be because a parabola is not a perfect approximation for the drop shape in the vicinity of the contact line.

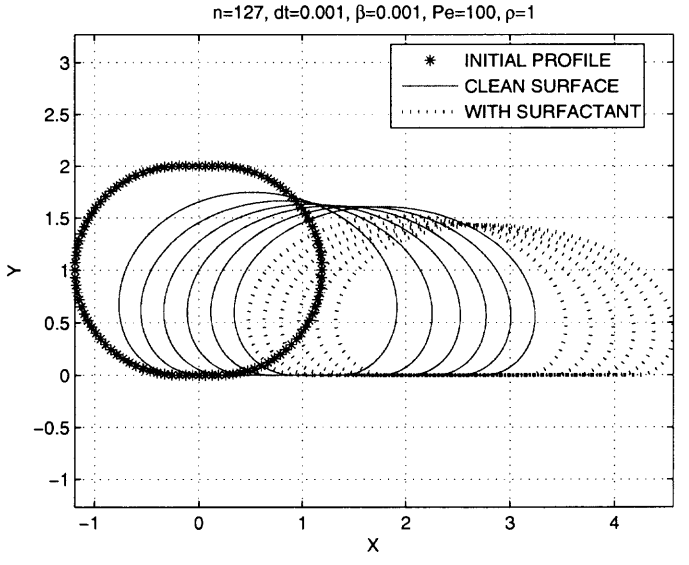


**Figure 3.27** Rolling drop with surfactant. $T = 0, 1, 2, 3, 4, 5, 6, 7, 8, 9, 10, 11, 12$.

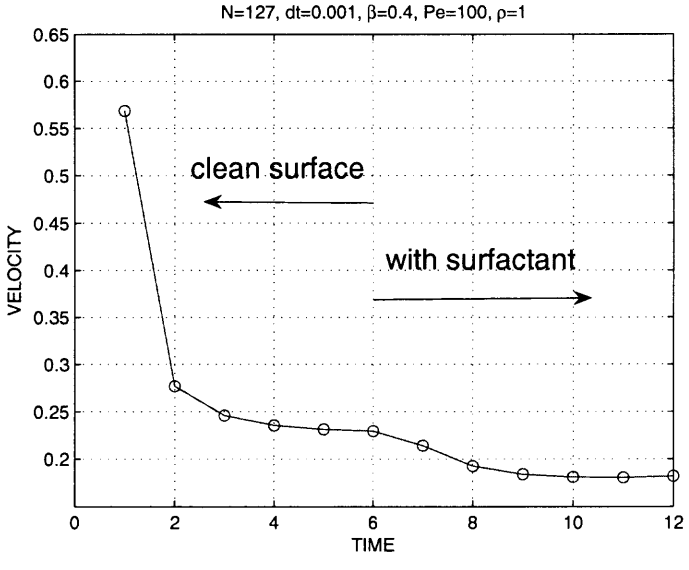


**Figure 3.28** A rolling drop with surfactant reaches a steady velocity.

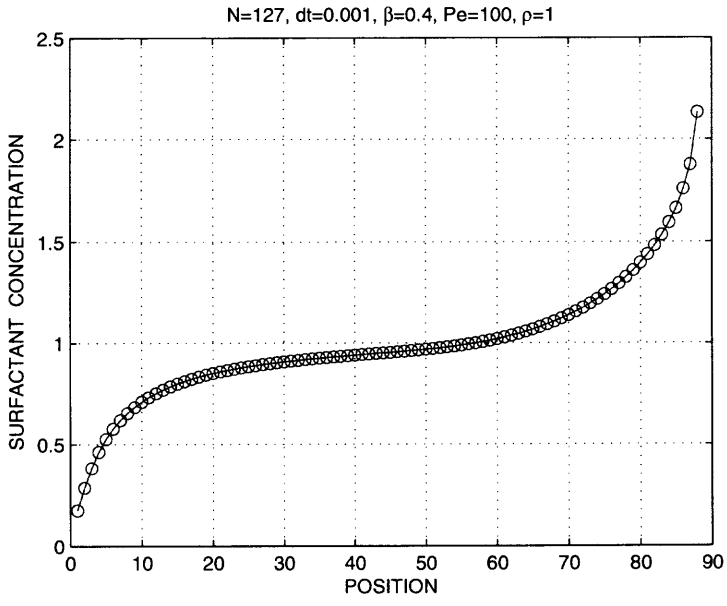


**Figure 3.29** Distribution of surfactant concentration at $T = 12$.

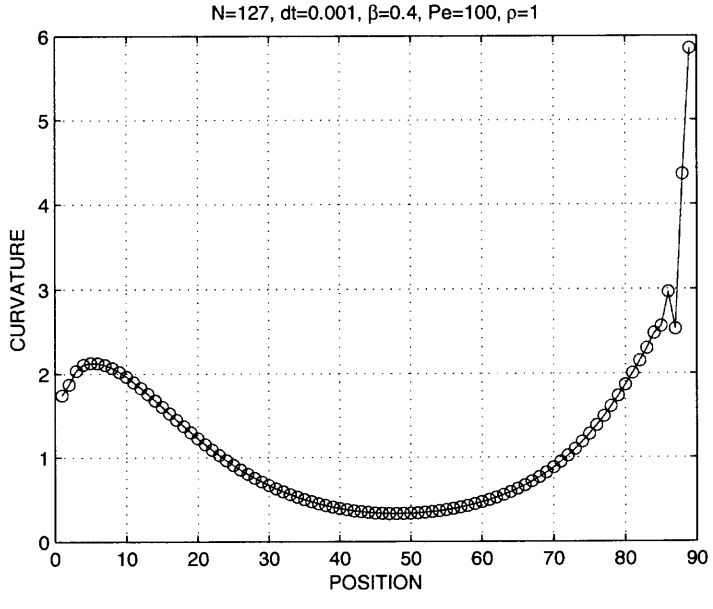


**Figure 3.30** The curvature of free surface at $T = 12$.

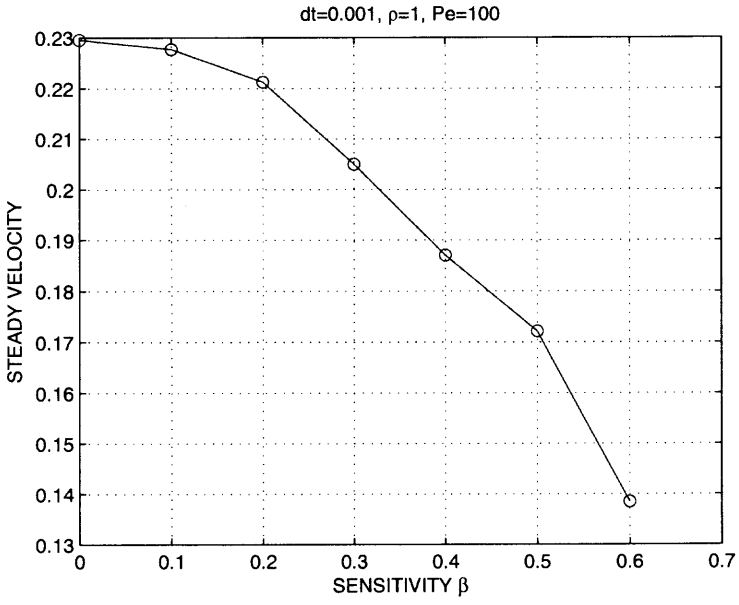


**Figure 3.31** The rolling motion is retarded due to the presence of surfactant.

In Figure 3.31, it shows when the sensitivity $\beta$ of surface is larger, the rolling motion is slower. From previous analysis for the clean drop, we know the steady velocity of large drop is linearly proportional to surface tension $\sigma$ (see Equation 3.71). This figure shows the steady velocity decreases not only because of the reduction of surface tension but also because of the counteraction of the Marangoni force since it is greater than linear decrease. In this numerical calculation, all parameters are equal to 1, and the sensitivity $\beta$ varies from 0 to 0.6.

# CHAPTER 4

# ASYMPTOTIC ANALYSIS IN THE VICINITY OF THE CONTACT LINE

## 4.1 Expansion in the Polar Coordinates

In this chapter, we are looking for a local non-singular solution without or with surfactant at the interface. As we mentioned before, there is a stress singularity at the contact line for a contact angle $\theta \in (0^0, 180^0)$ when usual hydrodynamic assumptions are applied. Several ways have been proposed to remove the singularity. One common way is to relax the boundary condition of no-slip at the solid. Another way, which has received much less attention, is to set the contact angle to be $180^0$. Previous work [11, 24] showed that the singularity is removed for the rolling motion (a $180^0$ contact angle) without a hydrostatic pressure term. There is a sign error in their analysis pointed out by Dussan [7] but the analysis is easily modified to acount for this. Mahadevan and Pomeau [25] considered the hydrostatic pressure term and derived the shape of the free surface and the stream function $\Psi$ in the vicinity of the contact point. Unfortunately they overlooked a balance in the Stokes equation. They derived their solution for the stream function from the biharmonic equation which is in turn derived from the Stokes equation. But the final result does not satisfy the Stokes equation with a constant (hydrostatic) pressure at leading order. We will go through all details in this chapter.

We start with Stokes equation in polar coordinate system as shown in Figure 4.1

$$\mu(\nabla^2 u_r - \frac{u_r}{r^2} - \frac{2}{r^2}\frac{\partial u_\theta}{\partial \theta}) = \frac{\partial p}{\partial r}, \tag{4.1}$$

$$\mu(\nabla^2 u_\theta + \frac{2}{r^2}\frac{\partial u_r}{\partial \theta} - \frac{u_\theta}{r^2}) = \frac{1}{r}\frac{\partial p}{\partial \theta}, \tag{4.2}$$

where the Laplace operator in the polar coordinate is

$$\nabla^2 = \frac{1}{r}\frac{\partial}{\partial r}(r\frac{\partial}{\partial r}) + \frac{1}{r^2}\frac{\partial^2}{\partial \theta^2}. \tag{4.3}$$

By writing velocity $u_r$ and $u_\theta$ associated with stream function,

$$\begin{aligned} u_r &= \frac{1}{r}\frac{\partial \Psi}{\partial \theta}, \\ u_\theta &= -\frac{\partial \Psi}{\partial r}. \end{aligned} \tag{4.4}$$

we obtain the Stokes equation in terms of stream function,

$$\mu(\frac{1}{r}\frac{\partial^3}{\partial r^2 \partial \theta} + \frac{1}{r^2}\frac{\partial^2}{\partial r \partial \theta} + \frac{1}{r^3}\frac{\partial^3}{\partial \theta^3})\Psi = \frac{\partial p}{\partial r}, \tag{4.5}$$

$$\mu(\frac{\partial^3}{\partial r^3} + \frac{1}{r}\frac{\partial^2}{\partial r^2} + \frac{1}{r^2}\frac{\partial^3}{\partial r \partial \theta^2} - \frac{1}{r^2}\frac{\partial}{\partial r} - \frac{2}{r^3}\frac{\partial^2}{\partial \theta^2})\Psi = -\frac{1}{r}\frac{\partial p}{\partial \theta}. \tag{4.6}$$

The no-slip boundary condition between fluid and solid substrate is

$$u_r = \frac{1}{r}\frac{\partial \Psi}{\partial \theta} = U, \tag{4.7}$$

$$\Psi = 0, \tag{4.8}$$

where $U$ is the boundary velocity.

At the free surface, there are basically three boundary conditions: tangential stress balance; normal stress balance; kinematic boundary condition. Tangential stress is balanced by the Marangoni force at the free surface $\theta = g(r)$,

$$\mu[(\frac{1}{r^2}\frac{\partial^2}{\partial \theta^2} + \frac{1}{r}\frac{\partial}{\partial r} - \frac{\partial^2}{\partial r^2})\Psi \cos 2\phi + 2(\frac{1}{r}\frac{\partial^2}{\partial r \partial \theta} - \frac{1}{r^2}\frac{\partial}{\partial \theta})\Psi \sin 2\phi] = -\overrightarrow{t} \cdot \nabla_s(\sigma). \tag{4.9}$$

Normal stress is balanced by the surface tension,

$$-p - 2\mu(\frac{1}{r}\frac{\partial^2}{\partial r \partial \theta} - \frac{1}{r^2}\frac{\partial}{\partial \theta})\Psi \cos 2\phi + \mu(\frac{1}{r^2}\frac{\partial^2}{\partial \theta^2} + \frac{1}{r}\frac{\partial}{\partial r} - \frac{\partial^2}{\partial r^2})\Psi \sin 2\phi = -\sigma\kappa. \tag{4.10}$$

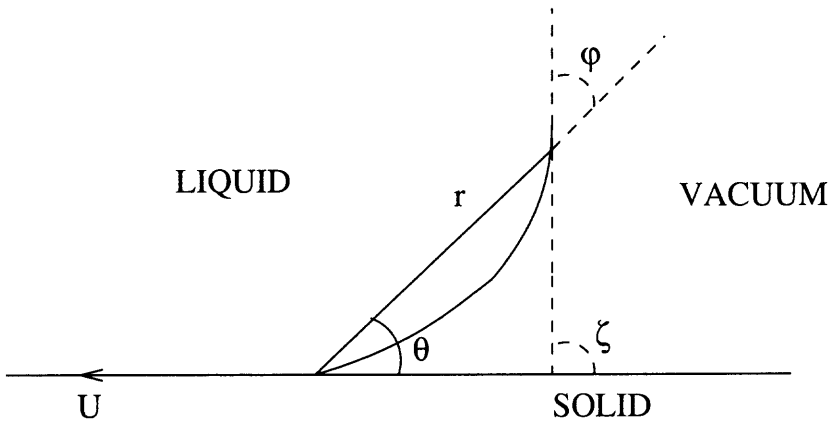


**Figure 4.1** The shape of free surface in the vicinity of contact line.

The operator in the right hand side of tangential stress balance equation (4.9) is

$$\vec{t} \cdot \nabla_s \sigma = \frac{\partial \sigma}{\partial s} = \frac{1}{\sqrt{r'^2 + r^2}} \frac{\partial \sigma}{\partial \theta} = \frac{1}{\sqrt{1 + r^2 \theta'^2}} \frac{\partial \sigma}{\partial r} = -\frac{\sigma_0 \beta \Gamma_r}{\Gamma_0 \sqrt{1 + r^2 \theta'^2}} \tag{4.11}$$

The dependence of surface tension $\sigma$ on surfactant concentration $\Gamma$ is

$$\sigma = \sigma_0 (1 - \beta \frac{\Gamma}{\Gamma_0}), \tag{4.12}$$

where $\Gamma_0$ is uniform initial surfactant concentration, $\sigma_0$ is surface tension of clean surface, and $\beta$ is the sensitivity parameter of surface tension to the surfactant concentration. The steady state equation for surfactant transport is

$$\frac{\partial (u_s \Gamma)}{\partial s} = D_s \frac{\partial^2 \Gamma}{\partial s^2}, \tag{4.13}$$

where $D_s$ is diffusivity of liquid surface, and $u_s$ is the velocity along the surface. Integrating along the surface, we obtain

$$u_s(0)\Gamma(0) - u_s \Gamma = D_s(0) \frac{\partial \Gamma(0)}{\partial s} - D_s \frac{\partial \Gamma}{\partial s}, \tag{4.14}$$

where the contact line is at $s = 0$. The diffusivity of solid is assumed to be 0 (i.e., $D_s(0) = 0$). The no-slip boundary condition says $u_s(0) = -U$. We assume a proportion $\Lambda$ of surfactant accumulated at the contact line streams onto the solid.

This means $u_s(0)\Gamma(0) = -U\Lambda\Gamma_0$ where $\Gamma_0$ is the amount of surfactant at the contact line.

$$-U\Lambda\Gamma_0 = u_s\Gamma - D_s\frac{\partial\Gamma}{\partial s}. \tag{4.15}$$

This equation can be read from the standpoint of conservation of surfactant. The left hand side is the flux of surfactant out of a "pillbox" centered at the contact point, and the right hand side represents the advective and diffusive flux into the "pillbox". In the steady state, the flux of surfactant is 0.

In Figure 4.1, the angle $\phi$ between the tangent line and the radial line satisfies (see Appendix C)

$$\tan\phi = \frac{r}{r'}. \tag{4.16}$$

Thus the surface velocity is

$$u_s = \frac{1}{\sqrt{r'^2 + r^2}}(r'u_r + ru_\theta) = \frac{1}{\sqrt{r'^2 + r^2}}(\frac{r'}{r}\frac{\partial\Psi}{\partial\theta} - r\frac{\partial\Psi}{\partial r}). \tag{4.17}$$

Therefore the steady state equation of surfactant transport becomes

$$-U\Lambda\Gamma_0 = \frac{1}{\sqrt{r'^2 + r^2}}(\frac{r'}{r}\frac{\partial\Psi}{\partial\theta} - r\frac{\partial\Psi}{\partial r})\Gamma - D_s\frac{1}{\sqrt{r'^2 + r^2}}\frac{\partial\Gamma}{\partial\theta}. \tag{4.18}$$

### 4.1.1 Dimensionless Equations

Next, nondimensionalize the above equations by the following characteristic parameters,

$$\begin{aligned}
\tilde{r} &= \frac{r}{L}, \\
\tilde{\Gamma} &= \frac{\Gamma}{\Gamma_0}, \\
\tilde{p} &= \frac{p}{\mu U/L}, \\
\tilde{\Psi} &= \frac{\Psi}{UL}.
\end{aligned} \tag{4.19}$$

where $U$ is the velocity of the moving boundary and $L$ is an arbitrary length. Then the non-dimensional Stokes equations (drop tildes) are

$$(\frac{1}{r}\frac{\partial^3}{\partial r^2\partial\theta}+\frac{1}{r^2}\frac{\partial^2}{\partial r\partial\theta}+\frac{1}{r^3}\frac{\partial^3}{\partial\theta^3})\Psi=\frac{\partial p}{\partial r}, \tag{4.20}$$

$$(\frac{\partial^3}{\partial r^3}+\frac{1}{r}\frac{\partial^2}{\partial r^2}+\frac{1}{r^2}\frac{\partial^3}{\partial r\partial\theta^2}-\frac{1}{r^2}\frac{\partial}{\partial r}-\frac{2}{r^3}\frac{\partial^2}{\partial\theta^2})\Psi=-\frac{1}{r}\frac{\partial p}{\partial\theta}. \tag{4.21}$$

Elimination of the pressure yields biharmonic equation,

$$(\frac{\partial^2}{\partial r^2}+\frac{1}{r}\frac{\partial}{\partial r}+\frac{1}{r^2}\frac{\partial^2}{\partial\theta^2})^2\Psi=0. \tag{4.22}$$

No-slip boundary condition at $\theta=\pi$,

$$u_r=\frac{1}{r}\frac{\partial\Psi}{\partial\theta}=1, \tag{4.23}$$

$$\Psi=0. \tag{4.24}$$

At the free surface $\theta=g(r)$, the tangential stress balance (TSB) is [11],

$$(\frac{1}{r^2}\frac{\partial^2}{\partial\theta^2}+\frac{1}{r}\frac{\partial}{\partial r}-\frac{\partial^2}{\partial r^2})\Psi\cos 2\phi+2(\frac{1}{r}\frac{\partial^2}{\partial r\partial\theta}-\frac{1}{r^2}\frac{\partial}{\partial\theta})\Psi\sin 2\phi=-\frac{1}{Ca\sqrt{1+r^2\theta'^2}}\frac{d\sigma}{dr}, \tag{4.25}$$

and the normal stress balance (NSB) is [11],

$$-p-2(\frac{1}{r}\frac{\partial^2}{\partial r\partial\theta}-\frac{1}{r^2}\frac{\partial}{\partial\theta})\Psi\cos 2\phi+(\frac{1}{r^2}\frac{\partial^2}{\partial\theta^2}+\frac{1}{r}\frac{\partial}{\partial r}-\frac{\partial^2}{\partial r^2})\Psi\sin 2\phi=-\frac{1}{Ca}\sigma\kappa, \tag{4.26}$$

where the capillary number $Ca=\frac{\mu U}{\sigma_0}$.

The dependence of surface tension on surfactant concentration is

$$\sigma=1-\beta\Gamma \tag{4.27}$$

The steady state equation of surfactant transport is,

$$-\Lambda=\frac{\Gamma}{\sqrt{r'^2+r^2}}(\frac{r'}{r}\frac{\partial\Psi}{\partial\theta}-r\frac{\partial\Psi}{\partial r})-\frac{1}{Pe}\frac{1}{\sqrt{r'^2+r^2}}\frac{\partial\Gamma}{\partial\theta}, \tag{4.28}$$

where the Peclet number $Pe = \frac{UL}{D_s}$. For the convenience in following analysis, all derivatives in equation 4.28 are expressed with respect to the radius $r$,

$$-\Lambda = \frac{\theta'\Gamma}{\sqrt{1+r^2\theta'^2}}\left(\frac{1}{\theta' r}\frac{\partial \Psi}{\partial \theta} - r\frac{\partial \Psi}{\partial r}\right) - \frac{1}{Pe}\frac{1}{\sqrt{1+r^2\theta'^2}}\frac{\partial \Gamma}{\partial r}. \tag{4.29}$$

### 4.1.2 Previous Work for Rolling Motion

We expand the variables in the following form,

$$\Psi = -r\sin\theta + r^q F_q(\theta) + \cdots, \tag{4.30}$$

$$\Gamma = 1 + br^s + \cdots, \tag{4.31}$$

$$\theta = g(r) = ar^t + \cdots. \tag{4.32}$$

In the expansion of stream function, the first term $r\sin\theta$ is derived from the no-slip boundary condition. The power $q$, $s$ and $t$ in the above expansion will be determined in the following procedure. First plugging the expansion of stream function in the biharmonic equation, we obtain

$$[q^2(q-2)^2F_q(\theta) + (q^2+(q-2)^2)F_q''(\theta) + F_q''''(\theta)]r^{q-4} = 0, \tag{4.33}$$

i.e.,

$$\left(\frac{d^2}{d\theta^2} + q^2\right)\left(\frac{d^2}{d\theta^2} + (q-2)^2\right)F_q(\theta) = 0. \tag{4.34}$$

Next we try to find the corresponding boundary conditions. First, the solid substrate is a stream line so the stream function is a constant (assume the constant is 0 without lost of generality) at $\theta = \pi$,

$$F_q(\pi) = 0. \tag{4.35}$$

The second one is the no-slip condition $u_r = 1$ at $\theta = \pi$ which implies,

$$-\cos\theta + r^{q-1}F_q'(\theta) = 1, \qquad \text{at} \qquad \theta = \pi, \tag{4.36}$$

i.e.,

$$F_q'(\pi) = 0. \tag{4.37}$$

The third one comes from the condition of stream function on the free surface $\theta = ar^t$. The free surface is a stream line since we consider the steady motion, i.e., $\Psi = 0$,

$$-ar^{t+1} + r^q F_q(0) = 0, \tag{4.38}$$

which requires

$$t = q - 1, \tag{4.39}$$

and leads to

$$-a + F_q(0) = 0. \tag{4.40}$$

Before we go to the normal stress balance and tangential stress balance, we need to solve the surfactant concentration. Substituting the expansion of stream function into the steady equation 4.29 of surfactant transport, we obtain,

$$-\Lambda\sqrt{1 + r^2\theta'^2} = [(-\cos\theta + r^{q-1}F_q'(\theta)) - a(q-1)r^{q-1}(-r\sin\theta + qr^{q-1}F_q(\theta))]\Gamma - \frac{1}{Pe}\frac{\partial\Gamma}{\partial r}. \tag{4.41}$$

As the radius $r$ goes to zero, the leading order is

$$-\Lambda = -\Gamma - \frac{1}{Pe}\frac{\partial\Gamma}{\partial r}. \tag{4.42}$$

We can find the solution of surfactant concentration with the boundary condition $\Gamma(0) = 1$,

$$\Gamma(r) = (1 - \Lambda)e^{-Per} + \Lambda \qquad \text{for} \qquad r \ll 1. \tag{4.43}$$

Thus the expansion of the surfactant concentration is,

$$\Gamma = 1 - Pe(1-\Lambda)r + \cdots . \tag{4.44}$$

In order to find the appropriate balances from the normal stress balance and the tangential stress balance, we need to consider these two boundary conditions together with pressure solved from the Stokes equation. First plug the expansion of stream function into the Stokes equations (4.20) and (4.21) and obtain

$$[q^2 F_q'(\theta) + F_q'''(\theta)] r^{q-3} = \frac{\partial p}{\partial r}, \tag{4.45}$$

$$[q^2(q-2)F_q(\theta) + (q-2)F_q''(\theta)] r^{q-3} = -\frac{1}{r}\frac{\partial p}{\partial \theta}. \tag{4.46}$$

The tangential stress balance is

$$r^{q-2}(F_q''(\theta) + q(2-q)F_q(\theta))\cos 2\phi + 2(q-1)r^{q-2}F_q'(\theta)\sin 2\phi = \frac{-\beta Pe(1-\Lambda)}{Ca\sqrt{1+r^2\theta'^2}}, \tag{4.47}$$

and the normal stress balance is

$$-p - 2(q-1)r^{q-2}F_q'(\theta)\cos 2\phi + r^{q-2}(F_q''(\theta) + q(2-q)F_q(\theta))\sin 2\phi = -\frac{1}{Ca}\sigma\kappa, \tag{4.48}$$

where the curvature

$$\kappa = \frac{rg''(r) + 2g'(r) + r^2(g'(r))^3}{(1 + r^2(g'(r))^2)^{3/2}}. \tag{4.49}$$

Since the leading order of $\theta = g(r)$ is

$$g(r) = ar^{q-1}, \tag{4.50}$$

then

$$g'(r) = a(q-1)r^{q-2}, \tag{4.51}$$

and

$$g''(r) = a(q-1)(q-2)r^{q-3}. \tag{4.52}$$

Therefore the curvature is

$$\kappa = \frac{[a(q-1)(q-2) + 2a(q-1)]r^{q-2} + a^3(q-1)^3 r^{3q-4}}{(1 + a^2(q-1)^2 r^{2q-2})^{3/2}} \tag{4.53}$$

Previous work for a clean surface by Mahadevan and Pomeau [25] showed that the hydrostatic pressure balances the capillary force in the vicinity of the contact line while the viscous force is not important in the normal stress balance. This requires that the curvature at the contact line should be constant in the leading order. This leads

$$q = 2. \tag{4.54}$$

It means that the free surface is a parabola

$$\theta = ar \qquad \text{or} \qquad y = ax^2. \tag{4.55}$$

They derived the stream function (replace $\frac{1}{2R}$ in their analysis with $2a$)

$$\Psi = -2ar^2 U(1 - \frac{\theta}{\pi} + \frac{\sin 2\theta}{2\pi}). \tag{4.56}$$

This stream function shows there is no singularity in either the force or the stress at the contact line. Unfortunately, they overlooked the Stokes equation (4.20). It is easy to verify this result is wrong by plugging this stream function into the Stokes equation (4.20). It ends up being

$$\frac{2U}{R\pi}\frac{1}{r} = \frac{\partial p}{\partial r}. \tag{4.57}$$

This cannot satisfy the condition of pressure being constant at the contact line.

Benney and Timson [11] found a non-singular solution for clean surface with a $180^0$ contact angle. The key difference of their work from that of Mahadevan and Pomeau is that the capillary force is balanced by the viscous force, and that the pressure is zero or infinite at the contact line. Therefore the hydrostatic term does not enter into the leading order balance. The pressure is solved from the Stokes equations. That is

$$p = \frac{r^{q-2}}{q-2}[q^2 F_q'(\theta) + F_q'''(\theta)]. \tag{4.58}$$

Then the leading order of the normal stress balance yields

$$-\frac{F_q'''(0) + (3q^2 - 6q + 4)F_q'(0)}{q-2} = -\frac{1}{Ca}q(q-1), \tag{4.59}$$

and the leading order of the tangential stress balance yields

$$F_q''(0) - q(q-2)F_q(0) = 0. \tag{4.60}$$

Their analysis ends up with the biharmonic equation (4.34) with five boundary conditions (4.35), (4.37), (4.40), (4.59) and (4.60). This eigenvalue problem yields an expression for q,

$$\tan q\pi = -2Ca. \tag{4.61}$$

For the local analysis for the rolling on motion with surfactant, we conclude there is no local steady state solution. The tangential stress balance equation (4.47) yields

$$q = 2. \tag{4.62}$$

This leads to non-bounded pressure at the contact line from the Stokes equation. The similar analysis to what Mahadevan & Pomeau did leads to a contradiction.

## 4.2 Lubrication Approximation at Contact Line

In order to justify our use of constant curvature at the contact line, we show that a parabolic interface shape with constant curvature and constant pressure at the contact line are consistent with the lubrication approximation. We consider the rolling motion of viscous flow without surfactant in the Cartesian coordinates under lubrication approximation. The contact line is at the origin. Assume

$$\epsilon = \frac{b}{L} \ll 1 \tag{4.63}$$

in the contact region. Then we non-dimensionalize the Stokes equations and boundary conditions by the following dimensionless variables

$$x' = \frac{x}{L},$$

$$y' = \frac{y}{\epsilon L},$$

$$u' = \frac{u}{U},$$

$$v' = \frac{v}{\epsilon U},$$

$$p' = \frac{pL}{\epsilon \sigma_0}.$$

Substitute into the system of equations and drop prime. Then the dimensionless Stokes equations are

$$\epsilon^2 u_{xx} + u_{yy} = \frac{\epsilon^3}{Ca} p_x, \tag{4.64}$$

$$\epsilon^2 v_{xx} + v_{yy} = \frac{\epsilon}{Ca} p_y. \tag{4.65}$$

The tangential stress balance is

$$\frac{1}{1+\epsilon^2 h_x^2}[\epsilon h_x(v_y - u_x) + (\frac{1}{\epsilon} u_y + \epsilon v_x)(1 - \epsilon^2 h_x^2)] = 0, \tag{4.66}$$

and the normal stress balance is

$$-\epsilon p + Ca\frac{2}{1+\epsilon^2 h_x^2}(\epsilon^2 h_x^2 u_x - h_x(u_y + \epsilon^2 v_x) + v_y) = \epsilon\frac{h_{xx}}{(1+\epsilon^2 h_x^2)^{3/2}}. \tag{4.67}$$

Rescale

$$Ca = Ca_0\epsilon^3, \tag{4.68}$$

the same idea as we did in Chapter 2. Then the leading order Stokes equations are

$$u_{yy} = \frac{1}{Ca_0}p_x, \tag{4.69}$$

$$p_y = 0. \tag{4.70}$$

The leading order of the equation of the tangential stress balance is

$$u_y = 0, \tag{4.71}$$

and the leading order of the equation of the normal stress balance is

$$p = h_{xx}. \tag{4.72}$$

If the pressure is constat $p = p_0$ in the contact region, we can solve the free surface shape in the contact region from the normal stress balance. That is a parabola

$$h(x) = \frac{p_0}{2}x^2, \tag{4.73}$$

which satisfies boundary conditions $h(0) = 0$ and $h'(0) = 0$. This local argument holds even when surfactant is incorporated. This shows a locally parabolic shape with constant pressure and linear surfactant concentration is consistent in lubrication approximation. Of course, in limit as $x$ and $y$ tend to the contact line, we have shown in equation (4.57) that the constant curvature and pressure solution is not

consistent with the governing equations. We find from our numerical simulations that the global solution is rather insensitive to precise nature of the surface shape in a **small** neighborhood of the contact line. We assert that enforcing a parabolic interface with constant curvature and pressure in neighborhood of the contact line is a reasonable choice, in view of the simplicity of enforcing this condition and its consistency with the lubrication approximation.

# CHAPTER 5

# CONCLUSION

In this thesis work, we first use a simplified mathematical model employing the lubrication approximation to check the influence of insoluble surfactant on the air entrainment during the coating process. When the surfactant is present on the interface as described in chapter 2, it accumulates at the contact line due to the surface convection. The nonuniform concentration distribution of surfactant results in a Marangoni force which is opposed to the flow direction. When the surface velocity driven by the moving solid boundary is large, the fluid drag on the interface (which is opposed by the Marangoni force) is large. We find that this leads to a critical velocity at which point the steady solution no longer exists. For the capillary number above this critical value, we expected but did not investigate the unsteady solution where the contact line moves along the solid boundary. This is associated with air entrainment. This suggests that the surfactant can play an important role in the air entrainment during the coating process and the stability of the moving contact line.

Secondly, we consider viscous droplets rolling down an inclined non-wettable plane. The biharmonic boundary element method is used to study this problem numerically. In the numerical calculation, a local shape of a parabola derived from the lubrication approximation is used to move both the advancing and receding contact lines. Numerical results match the theoretical prediction of [25] very well. The results show: $(a)$ the steady velocity is inversely proportional to the squared radius $R$ when the drop size is less than capillary length $(\frac{\sigma}{\rho g})^{1/2}$; $(b)$ the steady velocity does not depend on the radius $R$ when the drop size is larger than the capillary length $(\frac{\sigma}{\rho g})^{1/2}$ (where $\sigma$ is surface tension, $\rho$ is liquid density and $g$ is acceleration of gravity). When the surfactant is present on the surface of droplets, the steady velocity is retarded

by the reduction of surface tension and the Marangoni force due the nonuniform concentration distribution of surfactant. We also found numerical evidence that the stress singularity at the contact line is alleviated when the contact angle is $180^0$.

We have also performed a local analysis of solution to the the Stokes flow with normal stress balance, tangential stress balance and kinematic boundary condition at the free surface boundary. For the local analysis for the clean surface of rolling motion, we found a mistake in Mahadevan & Pomeau's analysis [25]. The stream function and the pressure they derived does not satisfy one balance in the Stokes equations. But the local shape of a parabola is consistent with the lubrication approximation. We conclude that Benney & Timson's solution [11] is the only local solution. Since the local shape is determined by the capillary number, it is difficult to apply it in the numerical calculation. In our numerical calculation, we use a parabolic shape because it is easier and satisfies the lubrication approximation. This works well since our numerical evidence shows that the stress singularity at the contact line is alleviated. For the flow with surfactant at the interface, we find that there is no local solution for the rolling on motion. In our numerical calculation, we pick a parabolic shape because it is consistent with lubrication approximation and it works well.

# APPENDIX A

## CURVATURE CALCULATION BY TANGENT ANGLES

In Figure A.1, the vector $t_i$, connecting two mid-points $p_{i-1}$ and $p_i$, refers to the tangential vector at the node $q_i$. We use $\frac{d\Theta_i}{ds_i}$ to calculate the curvature at the mid-point $p_i$, where $d\Theta_i$ is the angle between two tangents $t_i$ and $t_{i+1}$, and $ds_i$ is the arclength between $q_i$ and $q_{i+1}$. The similar way is used to calculate the curvature at all nodes $q_i$ through which I calculate the derivatives of the curvature at the mid-points.

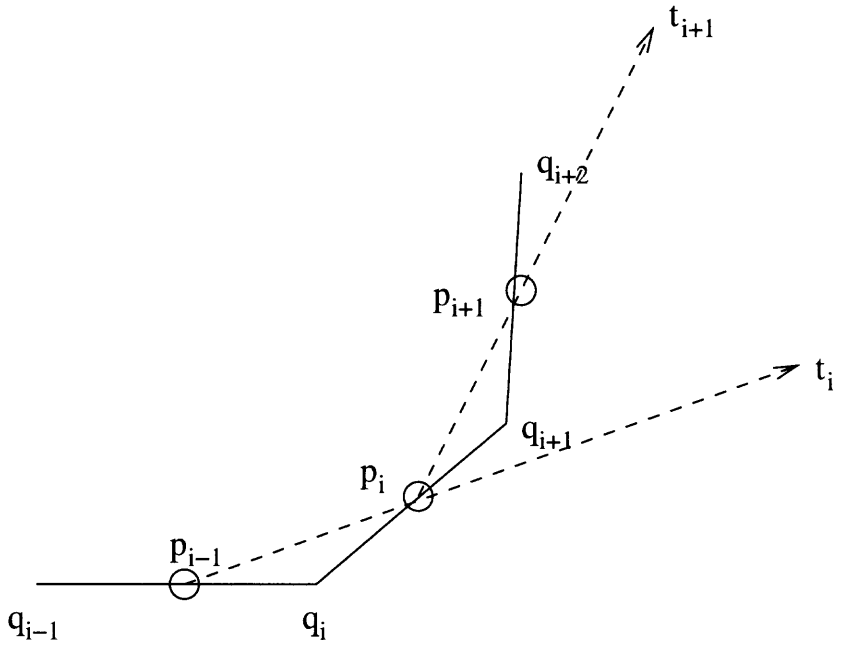


**Figure A.1** Geometry for curvature calculation. $p_i$ is a mid-point, and $q_i$ is a node.

# APPENDIX B

## CENTRAL SCHEME IN THE NON-EQUAL SPACING

Here are the centred schemes in the non-equal spacing for the derivative operators $\frac{\partial}{\partial s}$ and $\frac{\partial^2}{\partial s^2}$ where $s$ is the arc length of the boundary. All values such as $\frac{\partial \Psi}{\partial s}$ and $\frac{\partial^2 \Psi}{\partial s^2}$ are evaluated at the mid-points $p_i$.

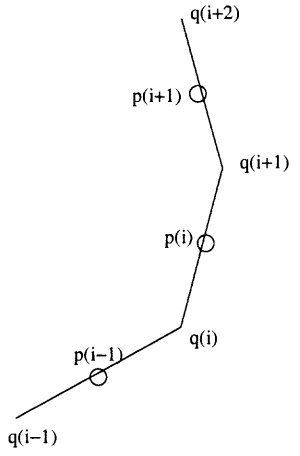


**Figure B.1** Boundary elements.

In figure B.1, $p_i$ is a mid-point and $q_i$ is a node. Define the arc length

$$s_i = |q_i - p_{i-1}| + |p_i - q_i|, \tag{B.1}$$

$$s_{i+1} = |q_{i+1} - p_i| + |p_{i+1} - q_{i+1}|. \tag{B.2}$$

The Taylor expansions of $\Psi_{i-1}$, $\Psi_i$ and $\Psi_{i+1}$ at $p_i$ are,

$$\Psi_{i-1} = \Psi_i - s_i \frac{\partial \Psi_i}{\partial s} + \frac{s_i^2}{2} \frac{\partial^2 \Psi_i}{\partial s^2} + O(s_i^3), \tag{B.3}$$

$$\Psi_i = \Psi_i, \tag{B.4}$$

$$\Psi_{i+1} = \Psi_i + s_{i+1} \frac{\partial \Psi_i}{\partial s} + \frac{s_{i+1}^2}{2} \frac{\partial^2 \Psi_i}{\partial s^2} + O(s_{i+1}^3). \tag{B.5}$$

The equation (B.3) multipling by $s_{i+1}^2$ substracts the equation (B.5) multipling by $s_i^2$, and add the equation (B.4) multipling by $(s_i^2 - s_{i+1}^2)$. The numerical scheme for the first derivative with respect to arc length $s$ is

$$\frac{\partial \Psi_i}{\partial s} \approx \frac{s_{i+1}^2 \Psi_{i-1} + (s_i^2 - s_{i+1}^2)\Psi_i - s_i^2 \Psi_{i+1}}{s_i s_{i+1}^2 - s_i^2 s_{i+1}}. \tag{B.6}$$

Similarly, the numerical scheme for the second derivative with respect to arc length $s$ is

$$\frac{\partial^2 \Psi_i}{\partial s^2} \approx \frac{s_{i+1}\Psi_{i-1} - (s_i + s_{i+1})\Psi_i + s_i \Psi_{i+1}}{(s_i^2 s_{i+1} + s_i s_{i+1}^2)/2}. \tag{B.7}$$

At the contact line, we use the one-side scheme to calculate the curvature at the free surface and the derivative operators. We use the values $\Psi_{i-1}$, $\Psi_i$, and $\Psi_{i+1}$ to calculate the value at $p_{i-1}$. The Taylor expansions of $\Psi_{i-1}$, $\Psi_i$ and $\Psi_{i+1}$ at $p_{i-1}$ are

$$\Psi_{i-1} = \Psi_{i-1}, \tag{B.8}$$

$$\Psi_i = \Psi_{i-1} + s_i \frac{\partial \Psi_{i-1}}{\partial s} + \frac{s_i^2}{2}\frac{\partial^2 \Psi_{i-1}}{\partial s^2} + O(s_i^3), \tag{B.9}$$

$$\Psi_{i+1} = \Psi_{i-1} + (s_i + s_{i+1})\frac{\partial \Psi_{i-1}}{\partial s} + \frac{(s_i + s_{i+1})^2}{2}\frac{\partial^2 \Psi_{i-1}}{\partial s^2} + O((s_i + s_{i+1})^3). \tag{B.10}$$

The equation (B.9) multipling by $(s_i + s_{i+1})^2$ substracts the equation (B.10) multipling by $s_i^2$, and then adds the equation (B.8) multipling by $(s_i^2 - (s_i + s_{i+1})^2)$. Therefore the one-side numerical scheme for the first derivative with respect to arc length $s$ is

$$\frac{\partial \Psi_{i-1}}{\partial s} \approx \frac{(s_i^2 - (s_i + s_{i+1})^2)\Psi_{i-1} + (s_i + s_{i+1})^2 \Psi_i - s_i^2 \Psi_{i+1}}{s_i(s_i + s_{i+1})^2 - (s_i + s_{i+1})s_i^2)} \tag{B.11}$$

Similarly, the one-side numerical scheme for the second derivative with respect to the arc length $s$ is

$$\frac{\partial^2 \Psi_{i-1}}{\partial s^2} \approx \frac{(s_i - (s_i + s_{i+1}))\Psi_{i-1} + (s_i + s_{i+1})\Psi_i - s_i \Psi_{i+1}}{((s_i + s_{i+1})s_i^2 - (s_i + s_{i+1})^2 s_i)/2}. \tag{B.12}$$

## APPENDIX C

## THE ANGLE BETWEEN THE TANGENT LINE AND THE RADIAL LINE

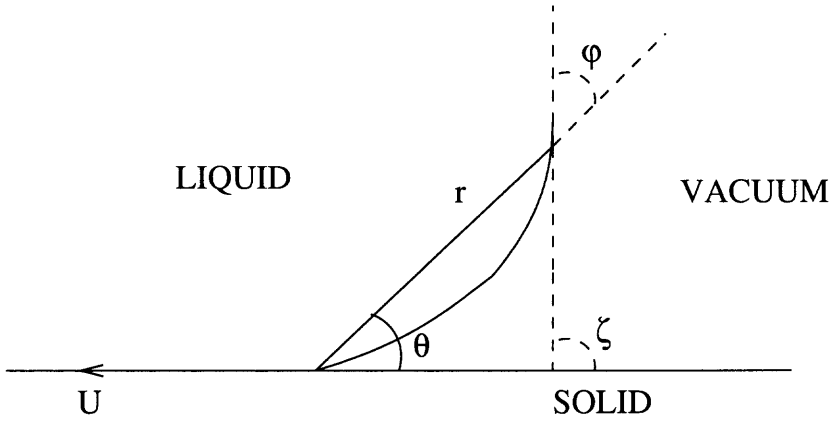


**Figure C.1** The relationship between $\phi$ and $\theta$.

In this figure, the free surface is $\theta = g(r)$. $\phi$ is the angle between the tangent line and the radial line. We will show

$$\tan\phi = r\theta' = \frac{r}{r'}. \tag{C.1}$$

In the polar coordinate system, the slope of the tangent line is

$$\tan\zeta = \frac{dy}{dx} = \frac{r'\sin\theta + r\cos\theta}{r'\cos\theta - r\sin\theta}. \tag{C.2}$$

Notice that $\phi = \zeta - \theta$, then

$$\begin{aligned}
\tan\phi &= \tan(\zeta - \theta) \\
&= \frac{\tan\zeta - \tan\theta}{1 + \tan\zeta\tan\theta} \\
&= \left(\frac{r'\sin\theta + r\cos\theta}{r'\cos\theta - r\sin\theta} - \tan\theta\right)\Big/\left(1 + \frac{r'\sin\theta + r\cos\theta}{r'\cos\theta - r\sin\theta}\tan\theta\right) \\
&= \frac{r}{r'}
\end{aligned} \tag{C.3}$$

## REFERENCES


[1] A. Mazouchi, C. M. Bramlich and G. M. Homsy, Time-dependent free surface Stokes flow with a moving contact line. 1. Flow over plane surfaces, *Physics of Fluids*, vol. 16, no. 5, 2004.

[2] L. K. Antanovskii, Formation of a pointed drop in Taylor's four-roller mill, *J. Fluid Mech.*, vol. 327, pp. 235-241, 1996.

[3] A. D. Schleizer and R. T. Bonnecaze, Displacement of a two-dimensional immiscible droplet adhering to a wall in shear and pressure-driven flows, *J. Fluid Mech.*, vol. 383, pp. 29-54, 1999.

[4] C. Neinhuis and W. Barthlott, Characterization and distribution of water-repellent, self-cleaning plant surfaces, *Annals of Botany*, vol. 79, pp. 667-677, 1997.

[5] C. D. Eggleton, E. Tsai and K. J. Stebe, Tip streaming from a drop in the presence of surfactants, *Physical Review Letters*, vol. 87, no. 4, 2001.

[6] C. Huh and L. E. Scriven, Hydrodynamic model of steady movement of a solid/liquid/fluid ccontact line, *Journal of Colloid and Interface Science* , vol. 36, no. 1, 1971.

[7] C. G. Ngan and E. B. Dussan V., The moving contact line with a $180^0$ advancing contact angle, *Physics of Fluids*, vol. 24, no. 12, 1984.

[8] D. Richard and D. Quere, Viscous drops rolling on a tilted non-wettable solid, *Europhys. Lett.*, vol. 48, no. 3, pp. 286-291, 1999.

[9] E. B. Dussan V. and S. H. Davis, On the motion of a fluid-fluid interface along a solid surface, *J. Fluid Mech.*, vol. 65, pp. 71-95, 1974.

[10] E. Rame, The spreading of surfactant-laden liquids with surfactant transfer through the contact line, *J. Fluid Mech.*, vol. 440, pp. 205-234, 2001.

[11] D. J. Benney and W. J. Timson, The rolling motion of a viscous fluid on and off a rigid surface, *Studies in Applied Mathematics*, vol. 63, pp. 93-98, 1980.

[12] F. Brochard-Wyart, H. Hervet, C. Redon and F.Rondelez, Spreading of "heavy" droplets 1. Theory, *Journal of Colloid and Interface Science*, vol. 142, No. 2, 1991.

[13] F. Chang, Y. Sheng, H. Chen and H. Tsao, From superhydrophobic to superhydrophilic surfaces tuned by surfactant solutions, *Applied Physics Letter* **91**, 094108, 2007.

[14] H. K. Moffatt,Viscous and resistive eddies near a sharp corner, *J. Fluid Mech.*, vol 18, pp. 1-18, 1964.

[15] H. K. Kuiken, Viscous sintering: the surface-tension-driven flow of a liquid form under the influence of curvature gradients at its surface, *J. Fluid Mech.*, vol. 214, pp. 503-515, 1990.

[16] H. A. Stone and L. G. Leal, The effects of surfactants on drop deformation and breakup, *J. Fluid Mech.*, vol. 220, pp. 161-186, 1990.

[17] H. Wong, D. Rumschitzki and C. Maldarelli, On the surfactant mass balance at a deforming fluid interface, *Physics of Fluids A*, vol. 8, pp. 3203-3204, 1996.

[18] J. Zhang, M. J. Miksis and S. G. Bankoff, Nonlinear dynamics of a two-dimensional viscous drop under shear flow, *Physics of Fluids*, 18(7), Art. no. 072106, 2006.

[19] J. A. Moriarty and L. W. Schwartz, Effective slip in numerical calculations of moving-contact-line problems, *Journal of Engineering Mathematics*, vol. 26, pp. 81-86, 1992.

[20] J. Jeong and H. K. Moffatt, Free-surface cusps associated with flow at low Reynolds number, *J. Fluid Mech.*, vol. 241, pp. 1-22, 1992.

[21] J. C. Coyne and H. G. Elrod, Conditions for the Rupture of a Lubricating Film. Part1: Theoretical Model, *Journal of Lubrication Technology*, July, 1970

[22] J. Li, The effect of an insoluble surfactant on the skin friction of a bubble, *European Journal of Mechanics B/Fluids*, vol. 25, pp. 59-73, 2006.

[23] J. Zhang, The dynamics of a viscous drop with a moving contact line, Ph.D. dissertation, Applied Mathematics, Northwestern University, June 2003.

[24] L. M. Pismen and A. Nir, Motion of a contact line, *Phys. Fluids*, vol. 25, no. 3, 1982.

[25] L. Mahadevan and Y. Pomeau, Rolling droplets, *Physics of Fluids*, vol. 11, no. 9, 1999.

[26] L. M. Hocking, A moving fluid interface. Part 2. The removal of the force singularity by a slip flow, *J. Fluid Mech.*, vol. 79, pp. 209-229, 1977.

[27] M. Callies and D. Quere, On water repellency, *Soft Matter*, vol. 1, pp. 55-61, 2005.

[28] M. R. Booty and M. Siegel, Steady deformation and tip-streaming of a slender bubble with surfactant in an extensional flow, *J. Fluid Mech.*, vol. 544, pp. 243-275, 2005.

[29] M. A. Kelmanson, An integral equation method for the solution of singular slow flow problems, *JCP*, vol. 51, pp. 139–158, 1983.

[30] M. A. Kelmanson, Boundary integral equation solution of viscous flows with free surfaces, *Journal of Engineering Mathematics*, vol. 17, pp. 329-343, 1983.

[31] M. Hameed, M. Siegel, Y.-N. Young, J. Li, M. R. Booty and D. T. Papageorgiou, Influence of insoluble surfactant on the deformation and breakup of a bubble or thread in a viscous fluid, *J. Fluid Mech.*, vol. 594, pp. 307-340, 2008.

[32] M. Siegel, Influence of surfactant on rounded and pointed bubbles in 2-D Stokes flow, *SIAM J. Appl. Math*, vol. 59, pp. 1998-2007, 1999.

[33] M. Siegel, Cusp formation for time-evolving bubles in two-dimensional Stokes flow, *J. Fluid Mech.*, vol. 412, pp. 227-257, 2000.

[34] M. A. Clay and M. J. Miksis, Effects of surfactant on droplet spreading, *Physics of Fluids*, vol. 16, no. 8, 2004.

[35] M. Ferrari, F. Ravera, S. Rao and L. Liggieri, Surfactant adsorption at superhydrophobic surfaces, *Applied Physics Letter*, **89**, 053104, 2006.

[36] P. Aussillous and D. Quere, Shapes of rolling liquid drops, *J. Fluid Mech.*, vol. 512, pp. 133-151, 2004.

[37] P. G. Simpkins and V. J. Kuck, Air entrapment in coatings by way of a tip-streaming meniscus, *Letters to nature*, vol. 403, pp. 641-643, 2000.

[38] R. Goodwin and G. M. Homsy, Viscous flow down a slope in the vicinity of a contact line, *Phys. Fluids A*, vol. 3, issue 4, pp. 515-528 1991.

[39] R. W. Hopper, Plane Stokes flow driven by capillarity on a free surface, *J. Fluid Mech.*, vol. 213, pp. 349-375, 1990.

[40] S. A. Kas-Danouche Rojas, Nonlinear interfacial stability of core-annular film flows in the presence of surfactants, Ph.D. dissertation, Applied Mathematics, New Jersey Institute of Technology, Newark, NJ, May 2002.

[41] S. Betelu, J. Diez, L. Thomas, R. Grantton and B. Marno, A Boundary Element Method for viscous Gravity Currents, *International Journal for Numerical Methods in Fluids*, vol. 25 pp. 1-19, 1997.

[42] S. N. Reznik and A. L. Yarin, Spreading of a viscous drop due to gravity and capillarity on a horizontal or an inclined dry wall, *Physics of Fluids*, vol. 14, no. 1, 2002.

[43] S. S. Sadhal and R. E. Johnson, Stokes flow past bubbles and drops partially coated with thin films. Part 1. Stagnant cap of surfactant film - exact solution, *J. Fluid Mech.*, vol. 126, pp. 237-250, 1983.

[44] V. M. Starov, S. R. Kosvintsev and M. G. Velarde, Spreading of surfactant solutions over hydrophobic substrates, *Journal of Colloid and Interface Science*, vol. 227, pp. 185-190, 2000.

[45] W. Barthlott and C. Neinhuis, Purity of the sacred lotus, or escape from contamination in biological surfaces, *Planta*, vol. 202, pp. 1-8, 1997.

[46] W.-Q. Lu, and H.-C. Chang, An extension of the Biharmonic Boundary Integral Method to free surface flow in channels," *JCP*, vol. 77, pp. 340-360, 1988.